https://doi.org/10.5194/egusphere-2023-706
Preprint. Discussion started: 26 April 2023

Oceanographic Processes Favoring Deoxygenation Inside Patagonian Fjords

Pamela Linford[1,2], Iván Pérez-Santos[2,3,4,*], Paulina Montero[3,4], Patricio Díaz[2,5], Claudia Aracena[6,7], Elías Pinilla[8,13], Facundo Barrera[2,9,10], Manuel Castillo[11], Aida Alvera-Azcárate[12], Mónica Alvarado[13], Gabriel Soto[8], Cécile Pujol[12], Camila Schwerter[2], Sara Arenas-Uribe[2], Pilar Navarro[2], Guido Mancilla-Gutiérrez[2], Robinson Altamirano[2], Javiera San Martín[7], Camila Soto-Riquelme[8].

[1]Programa de Doctorado en Ciencias, Mención Conservación y Manejo de Recursos Naturales, Universidad de Los Lagos, Puerto Montt, Chile.
[2]Centro i-mar, Universidad de Los Lagos, Casilla 557, Puerto Montt, Chile.
[3]Center for Oceanographic Research COPAS Sur-Austral and COPAS COASTAL, Universidad de Concepción, Chile.
[4]Centro de Investigación en Ecosistemas de la Patagonia (CIEP), Coyhaique, Chile.
[5]CeBiB, Universidad de Los Lagos, Casilla 557, Puerto Montt, Chile.
[6]Centro de Investigación en Recursos Naturales y Sustentabilidad, Universidad Bernardo O'Higgins, Avenida Viel 1497, Santiago, Chile.
[7]Laboratorio Costero de Recursos Acuáticos de Calfuco, Universidad Austral de Chile, Valdivia, Chile.
[8]Instituto de Fomento Pesquero (IFOP), CTPA-Putemún, Castro, Chile.
[9]Centro de Ciencia del Clima y la Relicencia (CR2), Universidad de Chile, Chile.
[10]Centro Austral de Investigaciones Científicas (CADIC), CONICET, Bernardo Houssay 200, Ushuaia, Argentina.
[11]Centro de Observación Marino para estudios de riesgos del ambiente Costero, Universidad de Valparaiso, Chile.
[12]AGO-GHER, University of Liège, Belgium.
[13]Servicio Hidrográfico y Oceanográfico de la Armada de Chile.
[14]Department of Civil and Environmental Engineering, University of Maine, 5711 Boardman Hall, Orono, ME, USA.

Correspondence to: I. Pérez-Santos (ivan.perez@ulagos.cl), https://orcid.org/0000-0002-0184-1122.

Abstract

The dissolved oxygen (DO) levels of oceanic-coastal waters has decreased over the last decade owing to the increase in surface water temperature caused by climate change. In addition, biological and human activity in coastal zones, bays, and estuaries has contributed to the acceleration of current deoxygenation. The Patagonian fjord and channel system is one world region where low DO water (LDOW, 30%–60% oxygen saturation) and hypoxia conditions (<30% oxygen saturation, 2 ml L^{-1} or 89.2 µmol L^{-1}) is observed. An *in-situ* data set of hydrographic and biogeochemical parameters (2017 stations), collected from sporadic oceanographic cruises between 1970 and 2021,

https://doi.org/10.5194/egusphere-2023-706
Preprint. Discussion started: 26 April 2023

was used to quantify the mechanism involved in the presence of LDOW and hypoxic conditions in northern Patagonian fjords. Results denoted two main areas with LDOW (e.g., Puyuhuapi Fjord-Jacaf channel, Comau Fjord, and the Reloncaví estuarine system) extending from 25–400 m depth. Simultaneously, hypoxia was recorded in the Puyuhuapi Fjord, Jacaf Channel, and Quitralco Fjord. Quitralco registered the lowest values of DO (9.36 µmol L^{-1} and 1.6% oxygen saturation) of the entire Patagonian fjord system. Areas of LDOW and hypoxia coincided with the accumulation of inorganic nutrients. Water mass analysis confirmed the contribution of equatorial subsurface water in the advection of the LDOW to only the Puyuhuapi Fjord and Jacaf Channel. In addition, in Puyuhuapi Fjord, hypoxic conditions occurred when the community respiration rate (6.6 g C $m^{-2}d^{-1}$) exceeded the gross primary production estimate (1.9 g C $m^{-2}d^{-1}$) possibly due to the increased consumption of DO during the use of both autochthonous and allochthonous organic matter. Biogeochemical processes and circulation regimens also contribute to deoxygenation and will be part of the discussion of the present research.

1 Introduction

Hypoxic conditions and deoxygenation have expanded globally over the last decade along coastal zones and oceans (Schmidtko et al., 2017; Breitburg et al., 2018). While hypoxia is mostly attributed to anthropogenic processes, such as eutrophication (Díaz et al., 2001; Conley et al., 2009; Meire et al., 2013), deoxygenation occurs most prominently in the open ocean due to natural forcing (Oschlies et al., 2018; Garcon et al., 2019). However, the trend of deoxygenation has recently accelerated owing to the warming of oceans due to climate change. Therefore, for decades, the scientific community has been paying close attention to this issue because of the expected impacts on the survival, abundance, development, growth, reproduction, and behavior of the most important taxonomic groups at different stages of their life cycles, such as mollusks, crustaceans, and fish (Sampaio et al., 2021, Ekau et al., 2010; Batiuk et al., 2009; Vaquer-Sunyer y Duarte, 2008; Breitburg et al., 1997; Díaz y Rosenberg, 1995; Andrewartha and Birch, 1986; Davis, 1975), which could also affect all services provided to humans (Laffoley and Baxter, 2019).

Some examples of the impact of LDOW on biological behaviors are changes in the composition of benthic communities in prolonged periods of DO<4.2 ml L^{-1} (Hoos, 1973); negative impact on the growth and abundance of cod (3.6 ml L^{-1}; 70%), the limit of the distribution of sardine larvae (2.6 ml L^{-1}; 50%), the distribution of jellyfish (1.6 ml L^{-1}; 30%), the decrease of the abundance, swimming capacity and filtration of copepods (0.52 ml L^{-1}; 10%), described by Ekau et al., (2010). Additionally, oxygen deficiency affects the growth rate and feed conversion efficiency, and in some species, even increases the concentration of toxic substances (Davis, 1975). In a Patagonian fjord for rainbow trout (*Salmo gairdneri*) used in recreational fishing, values less than 50% saturation caused a reduction in swimming speed (Jones, 1971b) and altered respiration and metabolism (Kutty, 1968a). In the case of coho salmon (*Oncorhynchus kisutch*), a commonly farmed species, a growth rate proportional to the oxygen level was observed for saturations between 40% and 80% (Herrmann, 1958), and the hypoxia modulated the transcriptional immunological response (Martinez et al., 2020). Finally, Pérez–Santos et al. (2018) reported habitat reduction of

https://doi.org/10.5194/egusphere-2023-706
Preprint. Discussion started: 26 April 2023

microzooplankton in a Patagonian fjord (Puyuhuapi Fjord) due to the presence of hypoxic conditions at depths below 100 m.

Throughout the world's oceans, there are areas in which the dissolved oxygen (DO) is significantly lower than in well-oxygenated areas (such as <20 µM, ~ 0.4 mg L^{-1}, or 0.31 ml L^{-1} as shown by Breitburg et al., (2018). These areas are known as oxygen minimum zones (OMZs). Because of the upwelling associated with OMZs, which draws up nutrient-rich waters, they experience elevated surface primary production. OMZs result from organic matter degradation, weak water circulation, long residence times, and weak ventilation (Fuenzalida et al., 2009). The major ocean OMZs are located in the Eastern South Pacific, the Arabian Sea, the Bay of Bengal (Indian Ocean), the West Bering Sea, and the Gulf of Alaska, covering approximately 8% of the total ocean or approximately 30 million km^2 (Paulmier and Ruiz-Pino, 2009; Fuenzalida et al., 2009).

Along the Perú-Chile coastline, the Eastern South Pacific (ESP) OMZ extends poleward, diminishing its influence on the adjacent coast of the Patagonian fjord system (Silva et al., 2009). Recently, Linford et al. (2023) demonstrated poleward transport of hypoxic and LDOW of the Equatorial Subsurface water mass (ESSW) alongside the Patagonian region. As ESSW (originated in the Equatorial region) moves south, it passes throughout the OMZ, carrying oxygen-poor water (2−3 ml L^{-1}) with high nitrate concentration (20−30 µM) and elevated salinity (34.9) (Silva et al., 2009). Studies of water masses inside Patagonian fjords and channels have detected the presence of ESSW only in the northern region, between 41° S and 45° S. This water mass enters the northern Patagonia region via the Guafo mouth, a deep channel with a depth of 150−200 m and width of 35 km (Sievers and Silva, 2008; Pérez-Santos et al., 2014; Schneider et al., 2014). ESSW is one of the main causes of hypoxia and LDOW inside Patagonian fjords (e.g., Puyuhuapi Fjord and Jacaf Channel). Nevertheless, these conditions are also found in other areas far from the influence of ESSW, e.g., the Reloncaví system (Reloncaví Fjord and Reloncaví Sound), Aysén, Comau, and Quitralco fjords (Figure 1) (Silva and Vargas, 2014; Linford et al., 2023; Díaz et al., 2023).

Regarding other processes favoring hypoxia and LDOW inside Patagonian fjords, Silva (2008) proposed those biological processes that include the consumption of DO, such as respiration and the remineralization of organic matter. A high load of organic matter (autochthonous and allochthonous) in the water column and sediments increases DO consumption during microbial community respiration, contributing to the LDOW content in most of the Patagonian fjord headwaters (Castillo et al., 2016) as well as higher community respiration rates than primary production (Montero et al., 2011; Montero et al., 2017a). Weak deep ventilation and long residence times in fjord waters are also assumed to promote a reduction in the DO concentration (Schneider et al., 2014; Silva and Vargas, 2014).

Finally, most published manuscripts hypothesize and discuss the processes favoring deoxygenation inside Patagonian fjords but never show any quantification. The Patagonian fjord ecosystem is under substantial continued economic pressure, with salmon aquaculture occupying the first position, with a national production of ~1,000,000 tons of salmon in 2019 (Billi et al., 2022). The northern Patagonian fjord (a region similar to the study area; Figure 1b, 1c) reported half of the national production and a significant number of salmon concessions (Billi et al., 2022). A risk analysis carried out in this region established that the Reloncaví estuarine system, and the Comau, Puyuhuapi, Quitralco, and Cupquelan fjords are regions with an especially elevated level of risk for the development of harmful

https://doi.org/10.5194/egusphere-2023-706
Preprint. Discussion started: 26 April 2023

algal blooms (HABs) and eutrophication events, owing to the nutrients input by the intense aquaculture of salmon (Soto et al., 2021). Nevertheless, environmental studies on salmon farming have shown that this economic activity has a geographically limited impact, because most nutrients are quickly recycled by biological processes in the water column (Soto and Norambuena, 2004).

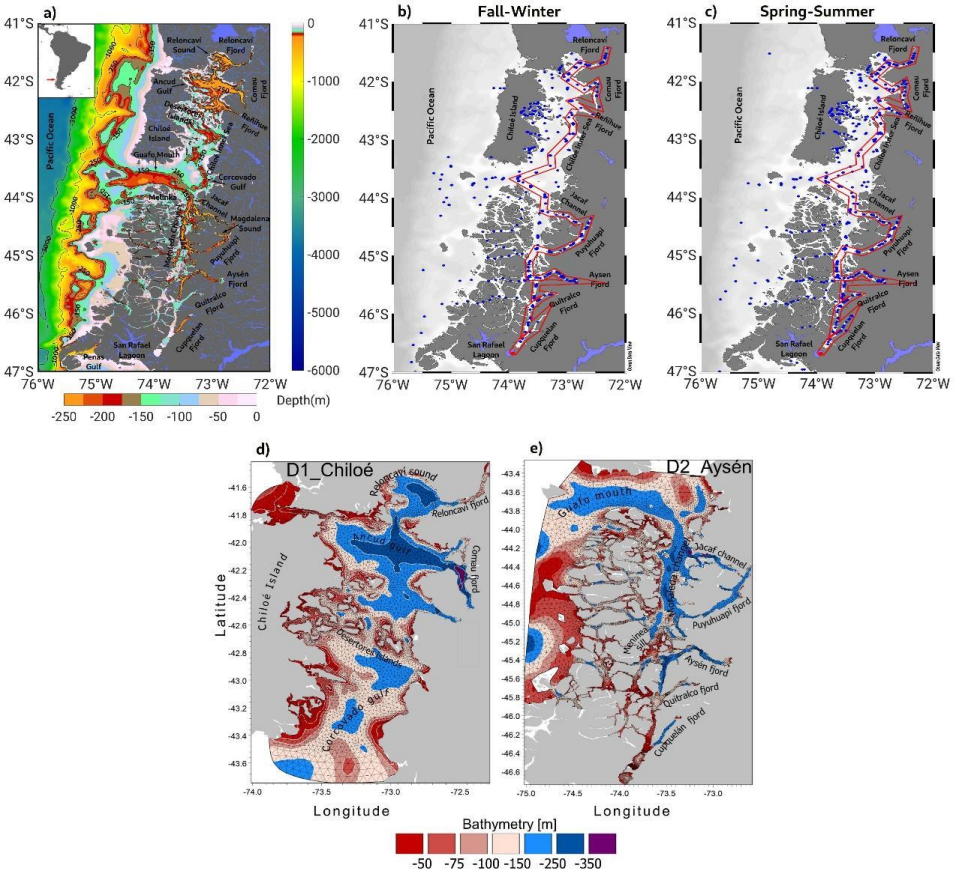

Figure 1. (a) Map showing the northern region of Patagonian fjords. Color bars represent bathymetric features from ETOPO2. (b, c) Sampling stations during the fall-winter and spring-summer seasons. Red lines in (b, c) represent along-fjord transect carried out to describe vertical features of hydrographic-biogeochemical stations from Figure 2. Data was collected on sporadic cruises, from 1970–2021 (see Table 1). (d, e) High-resolution model domain includes the northern Patagonia inner sea and is denoted as D1_Chiloé, while D2_Aysén covers the southern section. Bathymetry used was based on an SHOA nautical chart from the Chilean Navy.

Another meaningful impact of salmon production is the increase in allochthonous organic matter load, which, when combined with the high production of autochthonous organic matter by phytoplankton, favors a decrease in DO in the water column and sediments (Quiñones et al., 2019). Salmon farming supplies allochthonous dissolved substrates through the dissolution of organic particles derived from feces and uneaten feed (Wang et al., 2012). This

https://doi.org/10.5194/egusphere-2023-706
Preprint. Discussion started: 26 April 2023

organic material is considered highly degradable (Nimptsch et al., 2015; Montero et al., 2022), promoting enhanced rates of heterotrophic bacterial activity (e.g., bacterial production (BP) and extracellular enzymatic activity (EEA) (Montero et al., 2022).

The main goal of this study was to quantify the processes contributing to hypoxia and LDOW in northern Patagonia, such as ESSW advection, DO consumption during the use of organic matter (community respiration), biogeochemical processes, deep-water ventilation, and residence times of water inside fjords. An *in-situ* dataset of ~2000 profilers of hydrographic-chemical parameters was used to describe the seasonal distribution of water masses and their relationship with biogeochemical processes. Primary production experiments and the output of a 3D hydrodynamic model were utilized to demonstrate the occurrence of other processes involved in the deoxygenation of the northern Patagonian fjords.

2. Materials and Methods

2.1 Hydrographic and chemical data

A total of 2017 stations were used to describe northern Patagonia's hydrographical and chemical processes; 593 stations were sampled during the fall-winter seasons and 1424 during the spring-summer seasons (Table 1). Most temperature and salinity records were obtained using a CTD (Conductivity, Temperature, and Depth profiler) instrument (e.g., SBE19 plus, SBE15, and AML Metrec XL). Optical sensors and the Winkler method have been used to obtain DO data (Strickland and Parson, 1968). Figures 1b and 1c show the station positions during fall-winter and spring-summer. The absolute salinity (S_A in gkg^{-1}) and conservative temperature (Θ in °C) were calculated using the Thermodynamic Equation of Seawater 2010 (TEOS-10) (IOC et al., 2010). In TEOS-10, absolute salinity represents the spatial variation in the composition of seawater, considering the different thermodynamic properties and gradients of horizontal density in the open ocean. Conservative temperature is similar to potential temperature but represents the heat content of seawater with greater precision.

Table 1. Oceanographic campaigns carried out in Patagonian fjords and channels.

Expeditions	Date	Season	Stations	Measurements
HUDSON	06/03-01/04, 1970	Summer	112	(Temperature, Salinity) * + O2(bottle-Winkler) + Nutrients (PO4, NO3, Si; bottle)
CIMAR-01	18/10-04/11, 1995	Spring	99	CTD + O2(bottle-Winkler) + Nutrients (PO4, NO3, NO2, Si; bottle) + pH(bottle)
CIMAR-02	16/10-17/11, 1996	Spring	101	CTD + O2(bottle-Winkler) + Nutrients (PO4, NO3, Si; bottle) + pH(bottle)
CIMAR-04-I	28/09-09/10, 1998	Spring	31	CTD + O2(bottle-Winkler) + Nutrients (PO4, NO3, Si; bottle)
CIMAR-03	11-22/10/1998	Spring	59	CTD + O2(bottle-Winkler) + Nutrients (PO4, NO3, Si; bottle)
CIMAR-07-I	07-21/07/2001	Winter	49	CTD + O2(bottle-Winkler)
CIMAR-07-II	13-25/11/2001	Spring	51	CTD + O2(bottle-Winkler) + Nutrients (PO4, NO3, Si; bottle)
CIMAR-08-I	06-20/07/2002	Winter	51	CTD + O2(bottle-Winkler) + Nutrients (PO4, NO3, Si; bottle)

https://doi.org/10.5194/egusphere-2023-706
Preprint. Discussion started: 26 April 2023

CIMAR-08-II	16-24/11/2002	Spring	39	CTD + O2(bottle-Winkler) + Nutrients (PO4, NO3, Si; bottle)
CIMAR-09-I	09-23/08/2003	Winter	58	CTD + O2(bottle-Winkler) + Nutrients (PO4, NO3, Si; bottle)
CIMAR-09-II	07-20/11/2003	Spring	55	CTD + O2(bottle-Winkler) + Nutrients (PO4, NO3, Si; bottle)
CIMAR-10-I	26/06-31/08, 2004	Winter	49	CTD + O2(bottle-Winkler) + Nutrients (PO4, NO3, Si; bottle)
CIMAR-10-II	12-23/11/2004	Spring	63	CTD + O2(bottle-Winkler) + Nutrients (PO4, NO3, Si; bottle)
CIMAR-11-I	18-25/07/2005	Winter	78	CTD + O2(bottle-Winkler) + Nutrients (PO4, NO3, Si; bottle)
CIMAR-11-II	11-21/11/2005	Spring	80	CTD + O2(bottle-Winkler) + Nutrients (PO4, NO3, Si; bottle)
CIMAR-12-I	10-19/07/2006	Winter	32	CTD + O2(bottle-Winkler) +Nutrients (PO4, NO3, Si; bottle)
CIMAR-12-II	04-12/11/2006	Spring	40	CTD + O2(bottle-Winkler) + Nutrients (PO4, NO3, Si; bottle)
CIMAR-13-I	27/07-07/08, 2007	Winter	42	CTD + O2(bottle-Winkler) + Nutrients (PO4, NO3, Si; bottle)
CIMAR-13-II	02-12/11/2007	Spring	46	CTD + O2(bottle-Winkler) + Nutrients (PO4, NO3, Si; bottle)
CIMAR-14	01-19/11/2008	Spring	59	CTD + O2(bottle-Winkler) + Nutrients (PO4, NO3, Si; bottle)
CIMAR-15	09/10-09/11, 2009	Spring	51	CTD + O2(bottle-Winkler) + Nutrients (PO4, NO3, Si; bottle)
CIMAR-16	20/10-12/11, 2010	Spring	122	CTD + O2(bottle-Winkler) + Nutrients (PO4, NO3, Si; bottle)
CIMAR-17	17/10-14/11, 2011	Spring	195	CTD + O2(bottle-Winkler) + Nutrients (PO4, NO3, Si; bottle)
CIMAR-18	01/06-04/07, 2012	Fall-Winter	98	CTD + O2(bottle-Winkler) + Nutrients (PO4, NO3, Si; bottle)
CIMAR-19	04-16/07/2013	Winter	70	CTD + O2(bottle-Winkler) + Nutrients (PO4, NO3, Si; bottle)
CIMAR-20	04-22/10/2014	Spring	81	CTD + O2(bottle-Winkler) + Nutrients (PO4, NO3, Si; bottle)
CHEPU-IFOP	05-17/08/2017	Winter	22	CTD + O2(optic)
CIMAR-23	27/10-15/11, 2017	Spring	37	CTD + O2(optic) + Nutrients (PO4, NO3, Si; bottle)
CIMAR-24	26/09-16/10, 2018	Spring	37	CTD + O2(bottle-Winkler) + Nutrients (NO3; bottle)
CHEPU-MR-I	06-08/06/2018	Fall	12	CTD + O2(optic)
CHEPU-MR-II	11/10/2018	Spring	2	CTD + O2(optic)
PN-I (IFOP)	13-25/11/2020	Spring	32	CTD + O2(optic) + Nutrients (PO4, NO3, NO2, Si; bottle) + pH, Tur, Fluor (optic)
PN-II (IFOP)	24/02-04/03, 2021	Summer	32	CTD + O2(optic) + Nutrients (PO4, NO3, NO2, Si; bottle) + pH, Chl-a,Tur, Fluor(optic)
PN-III (IFOP)	28/07-10/08, 2021	Winter	32	CTD + O2(optic) + Nutrients (PO4, NO3, NO2, Si; bottle) + pH, Chl-a,Tur, Fluor (optic)

593 Fall-Winter + 1424 Spring-Summer = 2017 stations

2.2 Primary production, community respiration, bacterial production, and phytoplankton community.

https://doi.org/10.5194/egusphere-2023-706
Preprint. Discussion started: 26 April 2023

During the spring-summer period of 2020–2021 and summer of 2022, nine *in situ* experiments were conducted to measure gross primary production (GPP) and community respiration (CR) in some fjords of northern Patagonia (Table 2). Water samples were obtained from three depths (2, 10, and 20 m depth) at each sampling station. GPP and CR rates were estimated from changes in dissolved oxygen concentrations observed during *in situ* incubation of light and dark bottles (Strickland, 1960). Water from the Niskin bottles was transferred into 125 mL (nominal volume) borosilicate bottles (gravimetrically calibrated) using a silicone tube. Five time-zero bottles, five light bottles, and five dark bottles were used at each incubation depth. Water samples were collected at dawn and incubated throughout the entire light period. Time-zero bottles were fixed at the beginning of each experiment, whereas the light and dark incubation bottles were attached to the surface-tethered mooring system. The samples were incubated at the depths from which they were collected.

Dissolved oxygen concentrations were determined according to the Winkler method (Strickland and Parsons, 1968), using an automatic Metrohom burette (Dosimat plus 865) and automatic end-point detection (AULOX Measurement System). Daily GPP and CR rates were calculated as follows: GPP = (mean [O_2] light bottles – mean [O_2] dark bottles); CR = (mean [O_2] time zero bottles – mean [O_2] dark bottles). The GPP and CR values were converted from oxygen to carbon units using a conservative photosynthetic quotient of 1.25 (Williams and Robertson, 1991) and a respiratory quotient of 1.

A total of five bacterial production (BP) experiments were performed during the same period as mentioned above. Experiments were conducted using the same water samples collected for the *in situ* GPP and CR incubation experiments. The BP estimates were based on the incorporation of leucine into proteins using the microcentrifugation method (Smith and Azam, 1992). Briefly, a blank and three samples (1.5 mL) were taken from each sampling depth and incubated with L-[3,4,5-^{3}H]-leucine (123.8 Ci mmol^{-1}, 40 nM final concentration) in the dark for 1 h. After incubation, samples were extracted with 100% trichloroacetic acid (TCA), rinsed with 5% TCA, and centrifuged at 13500 rpm twice for 15 min before removal of the supernatant. Liquid scintillation cocktail Ecoscint (1 mL)(National Diagnostic) was added to each sample. The samples were counted for dpm using a Packard (Mod. 1600 TR) liquid scintillation counter. Discrete depth estimates of the GPP, CR, and BS rates were integrated to 20 m using the trapezoidal method.

For analyses of the phytoplankton community, water samples were collected from four discrete depths (2, 4, 10, and 20 m) using a 5 L Niskin bottle. Samples were stored in 120 mL clear plastic bottles and preserved in 1% Lugol's iodine solution (alkaline). From each sample, a 10 mL subsample was placed in a sedimentation chamber and allowed to settle for 12 h (Utermöhl, 1958) prior to identification at 40× and 100× under an inverted microscope (Carl Zeiss, Axio Observer A.1). Finally, taxonomic descriptions from Tomas (1997) were used to identify phytoplankton composition.

Table 2. *In situ* experiments were carried out in Patagonian fjords and channels. Gross primary production (GPP), community respiration (CR), and bacterial secondary production (BSP).

Fjord region	Date (mm-dd-yyyy)	Season	Measurements (g C m^{-2}d^{-1})			
			GPP	CR	BSP	GPP:CR

https://doi.org/10.5194/egusphere-2023-706
Preprint. Discussion started: 26 April 2023

*Reloncaví	02/27/2009	Summer	3.83	3.31	-	1.16
Compu	10/03/2020	Spring	1.22	0.92	0.06	1.32
Quitralco	11/17/2020	Spring	1.41	2.66	0.05	0.53
Camou	12/12/2020	Spring	0.12	1.67	0.15	0.07
Puyuhuapi	01/21/2020	Summer	1.89	6.64	0.25	0.28
Reloncaví	01/14/2021	Summer	2.60	1.90	0.58	1.37
Compu	03/19/2022	Summer	1.25	0.76	-	1.64
Quitralco	02/28/2022	Summer	0.73	1.71	-	0.42
Camou	03/16/2022	Summer	0.56	1.12	-	0.50
Puyuhuapi	01/20/2022	Summer	2.18	2.55	-	0.85

*Data were taken from Montero et al. (2011).

2.3. Satellite images

Sentinel-2 level 1 images were downloaded from the Copernicus Open Access Hub (https://scihub.copernicus.eu/) for specific dates and regions, as shown in Table 3. The chosen dates correspond to periods of high discharge of freshwater from the continent. Using ACOLITE v 20220222.0 (https://odnature.naturalsciences.be/remsem/software-and-data/acolite, (Vanhellemont and Rudick, 2018), we calculated suspended particulate matter following Nechad et al. (2016). These data have a spatial resolution of 10 m and allow the resolution of the small-scale distribution of suspended particulate matter within the narrow channels and fjords of the region.

Table 3. Dates and regions of the Sentinel-2 datasets analyzed.

Date	**Region**
17 March 2017	Puyuhuapi Fjord
09 May 2017	Reloncaví Sound and Fjord
06 April 2018	Comau Fjord
09 June 2022	Quitralco Fjord

2.4 Biogeochemical parameters and analysis

Biogeochemical parameters were collected in November 2020 (Expedition PN-I IFOP, Table 1). The water samples were obtained by filtering seawater collected (1−2 L) using a 25-mm diameter, GF/F filter (0.7µm pore diameter). Suspended particulate matter (SPM, µg L^{-1}), was determined by gravimetry using the weight difference between the dried filter and the same filter before filtration (Grasshoff et al., 2009). Particulate organic carbon (POC, µmol L^{-1}), total nitrogen (TN, µmol L^{-1}), stables carbon ($\delta^{13}C$, ‰) and nitrogen ($\delta^{15}N$, ‰) isotopes were obtained following the method described by Verardo et al., (1990), with modifications by Barrera et al., (2017) and Díaz et al., (2023), and measured at the Stable Isotope Facility at the Pontifical Catholic University of Chile by using an elemental analyzer (EA Flash 2000 Thermo Finnigan), interfaced to a continuous flow isotope ratio mass spectrometer (IRMS Delta V Advantage). We calculated the relative importance of allochthonous and autochthonous organic matter with two-source endmember mixing models (Bianchi, 2007). Given the fact that The autochthonous marine (f_M) and allochthonous terrestrial fractions (f_T) of organic carbon and nitrogen, respectively, sum to unity according to

$$\%POC_{terr} = \frac{(\delta.13C_s - \delta.13C_m)}{(\delta.13C_t - \delta.13C_m)}$$

where $\delta^{13}C_s$ is the isotopic composition of a sample, $\delta^{13}C_m$ is the marine endmember from more oceanic stations (-17 ‰), and $\delta^{13}C_t$ terrestrial is the riverine/lake endmember values for POC (-30 ‰) as proposed for this area by González

https://doi.org/10.5194/egusphere-2023-706
Preprint. Discussion started: 26 April 2023

et al., (2019). The carbon: nitrogen ratio was also calculated as a proxy for the organic matter pool (Barrera et al., 2017).

Dissolved inorganic nutrients (NO_3^-, NO_2^-, PO_4^{3-}, and $Si(OH)_4$) were analyzed from 15 mL seawater samples, stored at -20 ºC in HDPE bottles, using a Seal AA3 AutoAnalyzer according to the methodology described by Grasshoff et al., (1983) and standard methods for seawater analysis (Kattner and Becker, 1991). Chromophoric Dissolved Organic Matter (CDOM) was determined by fluorometry using quinine sulfate dihydrate (μgL^{-1} QSU) diluted in 0.1 N sulfuric acid at a specific wavelength (Ex/Em = 350/450 nm) as standard in a Trilogy Turner Design fluorometer and CDOM module (Kim et al., 2018).

2.5 Marine current register with ADCP

In the study region, three mooring systems were deployed in the Corcovado Gulf and Puyuhuapi Fjord (see Figure 9 for position). In each mooring, a Teledyne RD Instruments (TRDI) and a WorkHorse−300 kHz Acoustic Doppler Current Profiler (ADCP) were installed with the transducers facing downward. The instruments were configured with 1-m cell size and 1 h ensembles. The ADCP provides magnitude and direction (in Earth coordinates); thus, the current vector is decomposed into zonal (u) and meridional (v) components. The basic and standard protocol of quality control was applied to identify outliers and low-quality data following the methodology suggested by TRDI. To obtain the mean pattern of the zonal and meridional components of the currents, they were filtered using a low-pass cosine-Lanzcos filter of 121 weight and 40 h half-power.

2.6 Circulation model

To gain a better understanding of the physical forcing related to the DO dynamics, we used the hydrodynamic model MIKE 3 FM (DHI, 2019), which solves continuity, momentum, temperature, and salinity transport equations. Specific features of MIKE 3 FM, such as equations, parameterizations, and their numerical schemes, are described in the DHI, 2019. In this study, two high-resolution model domains include the North Patagonian inner sea named D1_Chiloé (41.3° S– 43.7° S) and D2_Aysén, with an area from 43.6°S to 46.8° S (Figures 1d, 1e). Bathymetry was based on SHOA nautical chart soundings, and a digital elevation model was constructed using the natural neighbor method (Sibson, 1981). This domain was discretized using triangular elements of different sizes. The highest resolution was observed in coastal, narrow, and shallow areas, with an average element size of ~300 m, whereas the spatial resolution near the boundary was ~1000 m.

The modeling period covered six years (2016–2021). The boundary conditions of temperature, salinity, currents, and sea level were based on CTD stations from different cruises conducted in the northern Patagonian fjords, most of which are included in Table 1. In addition, atmospheric forcings, such as wind stress and heat fluxes over the sea surface, were introduced using spatially and temporally varying fields from the WRF−IFOP (Weather Research and Forecasting Model of the Instituto Fomento Pesquero) atmospheric model. Finally, the performance of the WRF model was evaluated as described by Pinilla et al. (2020).

The freshwater sources were based on the FLOW-IFOP hydrological model, which uses precipitation and temperature series from the CR2MET gridded product (http://www.cr2.cl/datos-productos-grillados/) with a spatial

https://doi.org/10.5194/egusphere-2023-706
Preprint. Discussion started: 26 April 2023

resolution of 5 km × 5 km. Using this information, the runoff is simulated, and the daily discharge series is calculated. According to the information estimated by FLOW-IFOP, the average annual freshwater discharge entering domain D1_Chiloé was ~2545 $m^3 s^{-1}$, while in D2_Aysén it was 3126 $m^3 s^{-1}$ for the period 2016–2021, this includes the main rivers but also all those larger than the annual mean > 5 $m^3 s^{-1}$ supplied by FLOW-IFOP. The performance of the FLOW-IFOP model at the gauged river stations of the Chilean Water Authority (www.dga.cl) is available at http://chonos.ifop.cl/flow/.

Information from the hydrodynamic model MIKE 3 FM was used to calculate the flushing time by applying a conservative tracer. The flushing time, according to Takeoka (1984) and Monsen (2002), was defined as the time necessary for the total mass of material within an area of interest (fjord, sound, bay, etc.) to be reduced by a factor of e-1 (~37%) (Prandle, 1984). The initial concentration values assigned were 1 for the inner side and zero for the outer side of the area. During the simulation, the water mass from the original basin was gradually replaced by inputs from open boundaries and rivers. This variable represents the amount of the original water in each element within the domain of interest at a given time. Therefore, it can be expected to identify the less flushed areas within the modeled basins (Andrejev et al., 2004).

In the present study, the flushing time was implemented in the Ecolab module of the MIKE 3 FM for every fjord within D1_Chiloé and D2_Aysén. We validated the spatial salinity pattern in the hydrodynamics model using salinity as a proxy for water mass categories; therefore, when comparing the model and observations (CTD station) along North Patagonia showed good agreement, higher salinity (>33 kg^{-1}), associated with SAAW and ESSW ocean waters, enters the deep layer of the Guafo mouth, crosses the Corcovado Gulf, and ends its travel at the deep layers of the Puyuhuapi Fjord and Jacaf Channel. Furthermore, a decrease in salinity due to ice melting from the San Rafael Lagoon is also seen, which indicates the presence of estuarine water (EW) (See Figure S1).

3 Results

3.1. Long-term annual mean of hydrographic-chemical parameters

The long-term seasonal mean of conservative temperature denoted warmer water in the northern region (41.5°−43° S) during both seasons, between the Desertores Pass and the Reloncaví Fjord**.** In contrast, cold waters were observed in the deep layer of the Puyuhuapi Fjord and Jacaf Channel, but colder water was registered in San Rafael Lagoon. This location also had the lowest salinity (15–21 gkg^{-1}), indicating the presence of estuarine water (EW) owing to ice melting from the San Rafael Lagoon (Figure 2a-b). The EW moved from south to north and mixed with the Subantarctic oceanic water (SAAW), contributing to the origin of the Modified Subantarctic oceanic water (MSAAW), as was observed in the vertical-horizontal salinity distribution. The EW was also observed at the surface layer in the Reloncaví system all year round, but SAAW was presented especially during the fall-winter season. Finally, the Equatorial Subsurface water (ESSW) enters the deep layer of the Guafo mouth, crosses the Corcovado Gulf, and ends its travel at the deep layers of the Puyuhuapi Fjord and Jacaf Channel. During the fall-winter season, a slight reduction in ESSW distribution was observed (Figure 2c–d).

In the area contained by the ESSW, low DO (LDOW) and hypoxic waters were observed. Again, LDOW was registered at Reloncaví Fjord, but this time they were not related to the ESSW. The main seasonality difference

https://doi.org/10.5194/egusphere-2023-706
Preprint. Discussion started: 26 April 2023

highlighted the homogenization of the water column observed during the fall-winter seasons, in which high DO values (267−312 µmol L^{-1}) and oversaturated waters (< 100% DO Saturation) were registered in the Chiloé Inner Sea (CIS). Additionally, more extensions of the hypoxic conditions and LDOW were registered during the spring-summer seasons (Figure 2e–f).

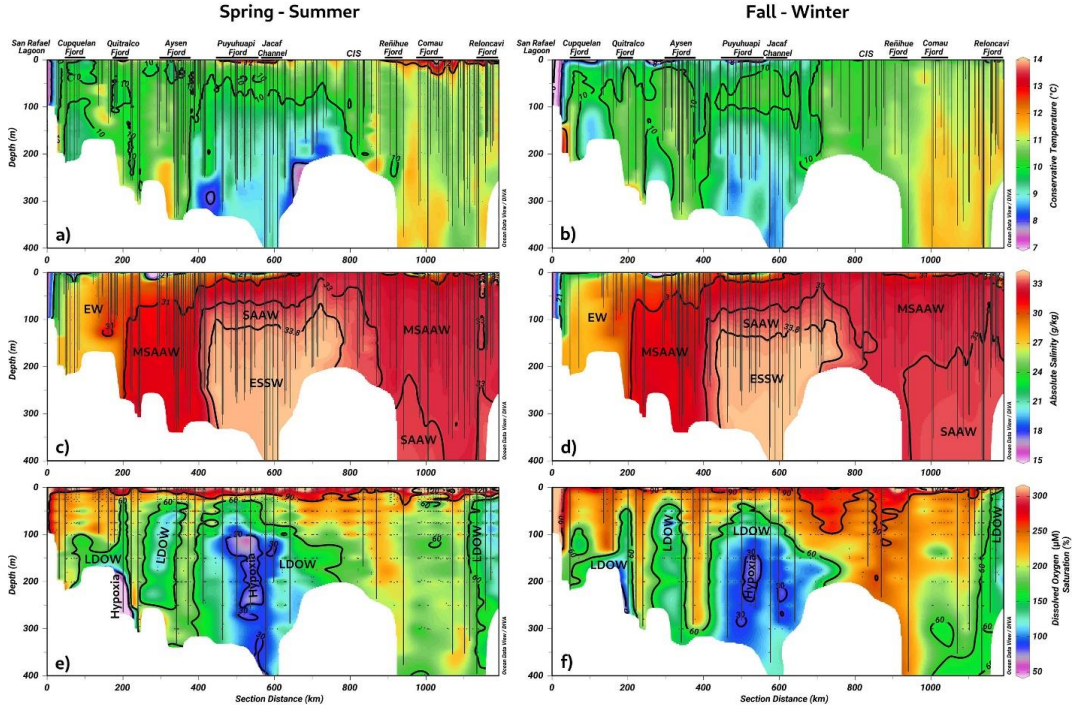

Figure 2. Long-term seasonal mean of hydrographic (a–d) and chemical (e–f) parameters collected along a vertical section in the northern Patagonian fjord during the fall-winter and spring-summer seasons.

As previously shown, the Puyuhuapi Fjord and Jacaf Channel were regions where high-salinity and hypoxic-LDOW waters were registered. In addition, a high concentration of inorganic nutrients was observed in the subsurface layer at a depth of 50 m (Figure 3). In the Puyuhuapi Fjord and the Jacaf Channel, between 100−300 m depth, nitrate (Figure 3a), phosphate (Figure 3c), and silicic acid (Figure 3e) range from 25–30 µM, 2–3 µM, and 30–50 µM, respectively. A second area with high inorganic nutrients was detected in the Reloncaví system, in which the highest absolute values of surface silicic acid were registered during the fall-winter season (e.g., 210 µM). Comparing seasonal concentrations, the fall-winter season showed the highest abundance in the water column. However, the absolute

https://doi.org/10.5194/egusphere-2023-706
Preprint. Discussion started: 26 April 2023

maximum nitrate (Figure 3b), phosphate (Figure 3d), and silicic acid (Figure 3f) values were recorded in the subsurface layer during the spring and summer seasons.

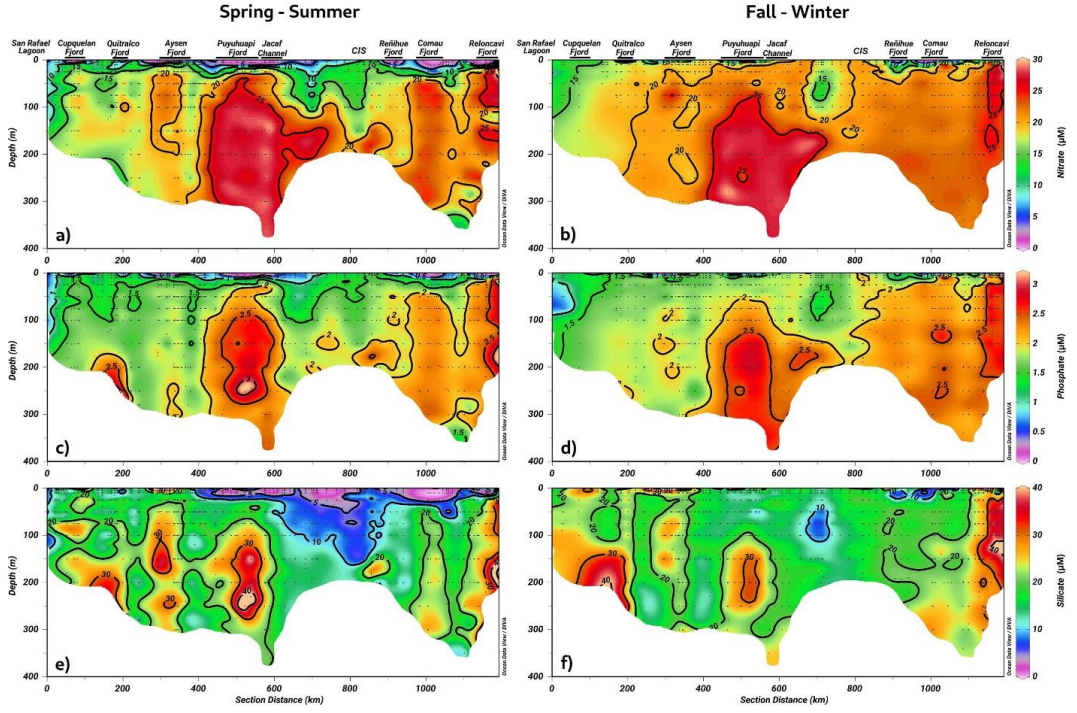

Figure 3. Long-term seasonal mean of inorganic nutrients. (a, b) Nitrate, (c, d) phosphate, and (e-f) silicate collected along a vertical section in the northern Patagonian fjord system during fall-winter and spring-summer seasons.

The analysis of hypoxia and LDOW conditions in the northern Patagonian fjord system highlighted the presence of two areas with water bodies with these characteristics, e.g., the Puyuhuapi-Jacaf and the Reloncaví regions. Moreover, Magdalena Sound (44.6° S / 72.9° W) showed shallower hypoxia over the entire Patagonian region. At this location, a 30% DO saturation isoline was observed at a depth of 70 m, and the LDOW reached a depth of approximately 20 m (Figure 4a-c). On another side, the lowest DO values of the northern Patagonian fjord system,

https://doi.org/10.5194/egusphere-2023-706
Preprint. Discussion started: 26 April 2023

specifically 9.36 µmol L^{-1} and 1.6% oxygen saturation, were recorded at the deepest layer (~200 m) of the Quitralco Fjord (45.7° S / 73.3° W) (Figure 4d–f).

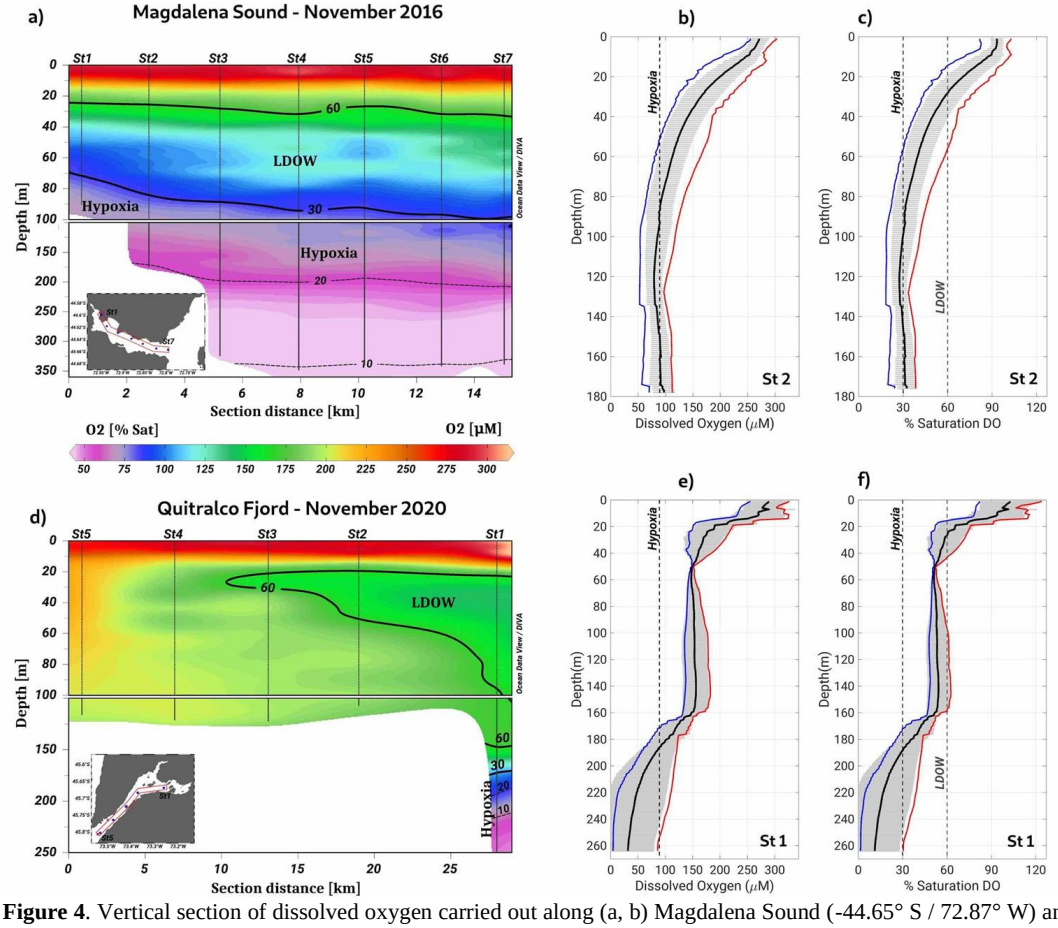

Figure 4. Vertical section of dissolved oxygen carried out along (a, b) Magdalena Sound (-44.65° S / 72.87° W) and (c, d) Quitralco Fjord during November 2016 and November 2020, respectively. In (b, c, e, f), red, black, and blue lines represent absolute maximum, average, and minimum values of the DO, respectively. The grey horizontal lines show the standard deviations calculated using 16 profiles for Magdalena Sound and 3 profiles for the Quitralco Fjord.

The calculation of the Brut-Väisälä frequency (BVF), a parameter used to identify mixed/stratified regions, evidenced a permanent mixing of the water column in the Chiloé inner sea (BVF>10 cycl h^{-1}) (Figure 5a–b). Furthermore, the homogenization of physical (e.g., conservative temperature and absolute salinity) and chemical (e.g., DO oxygen and inorganic nutrients) variables was observed in these regions. On another side, stratified water (between

https://doi.org/10.5194/egusphere-2023-706
Preprint. Discussion started: 26 April 2023

2 and 10 m depth) was detected during spring-summer inside the fjords, e.g., Cupquelan, Quitralco, Aysén, Puyuhuapi, Comau, and Reloncaví, showing values over BVF<50 cycl h^{-1} (Figura 5a).

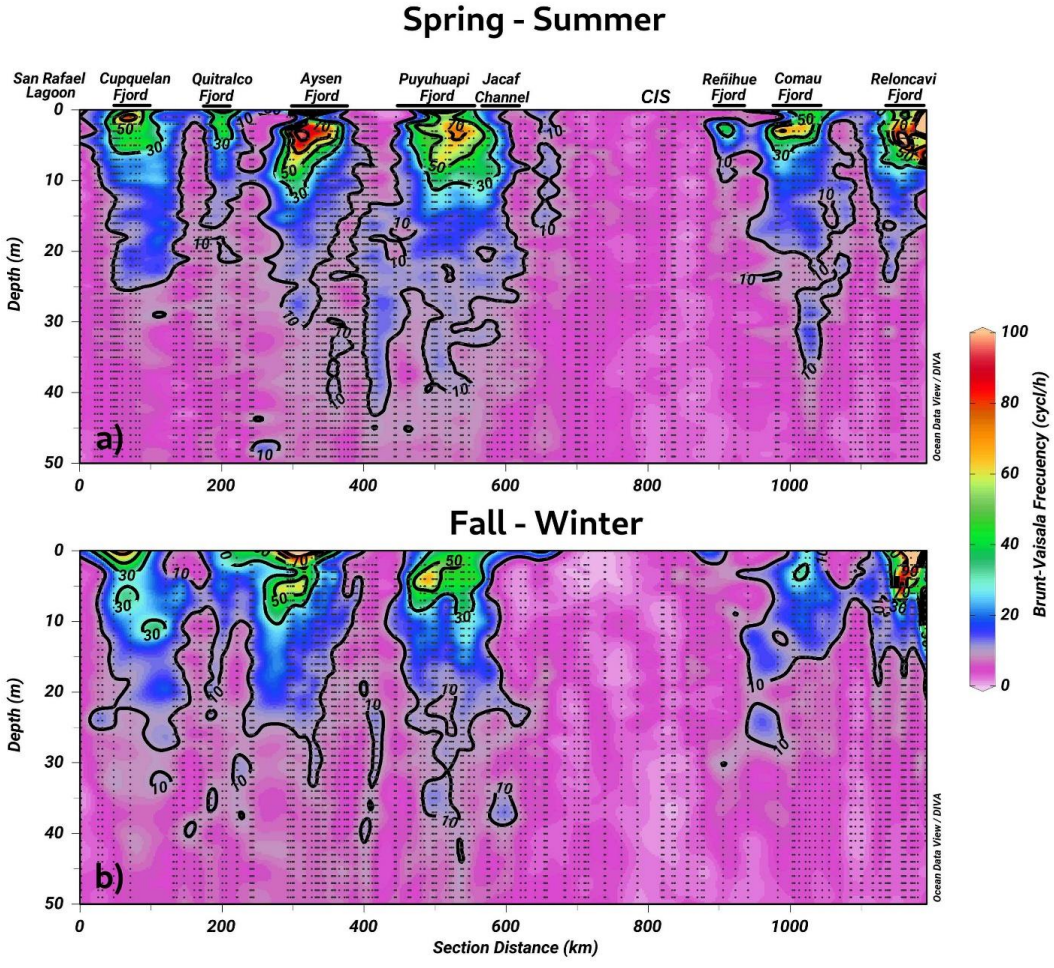

Figure 5. The long-term seasonal mean of Brut-Väisälä frequency along a vertical section in the northern Patagonian fjord during the (a) spring-summer, and (b) fall-winter seasons.

A comparison between oceanographic conditions measured in a similar station in Puyuhuapi Fjord (Figure 6), but 50 years apart, denoted deoxygenation of approximately -30−40 µmol L^{-1} registered from 50-150-m depth (Figure 6e–f). At the same layer, the conservative temperature decreased (~0.2 °C) (Figure 6a–b). Furthermore, the absolute salinity (Figure 6c–d) and inorganic nutrients, specifically, nitrate (~2 µmol L^{-1}) and phosphate (~0.5 µmol

https://doi.org/10.5194/egusphere-2023-706
Preprint. Discussion started: 26 April 2023

L^{-1}) increased (Figure 6g–j). A rate of increase of nutrient concentration by year can be estimated, in the case of nitrate, to be 0.04 µmol L^{-1} $year^{-1}$, and for phosphate, 0.01 µmol L^{-1} $year^{-1}$.

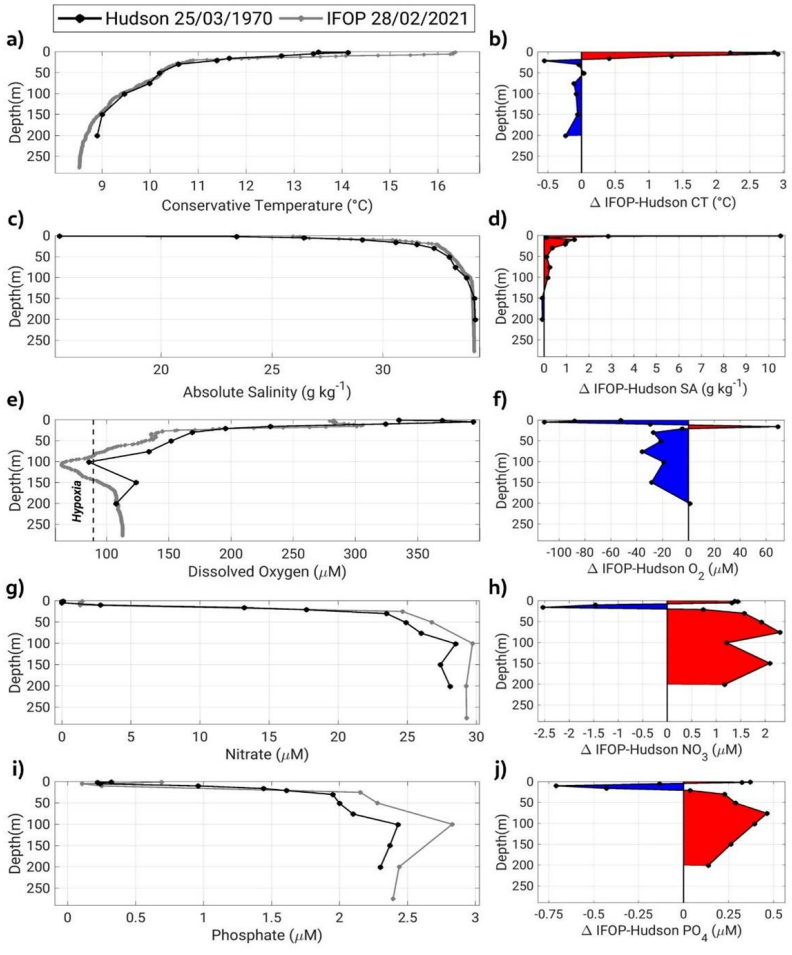

335 **Figure 6**. (a, c, e, g, i) Comparison of hydrographic and chemical profiles in a station located in Puyuhuapi Fjord (44.7° S/72.8° W) during the Hudson (March 25, 1970) and IFOP (February 28, 2021) oceanographic cruises. (b, d, f, h, j) show the difference between profiles.

3.2. Rates of primary production, community respiration, and bacterial production

Weak coupling was observed between the GPP and CR rates, with most experiments indicating that less
340 oxygen is produced than consumed (Figure 7a). Thus, most fjords exhibited heterotrophic metabolism (GPP:CR <1) in the surface layer (0–20 m) during the study period (Figure 7b). The highest rates of GPP in terms of oxygen (18.6 to 41.02 mmol O_2 m^{-3} d^{-1}) were mainly recorded in the upper 5 m of the water column, whereas the lowest values (0 to 17.6 mmol O_2 m^{-3} d^{-1}) were observed between 10 and 20 m depth (Figure 7c, 7j). CR rates did not show a definite

https://doi.org/10.5194/egusphere-2023-706
Preprint. Discussion started: 26 April 2023

vertical pattern, registering highest (23.3 to 76.3 mmol O_2 m^{-3} d^{-1}) and lowest (0 to 12.3 mmol O_2 m^{-3} d^{-1}) values throughout the water column (0–20 m) (Figure 7c, 7j).

Throughout the study period in different fjords, integrated GPP and CR rates (down to 20 m) ranged from 0.1–2.6 g C m^{-2} d^{-1} and from 0.8–6.6 g C m^{-2} d^{-1}, respectively, (Figure 8, Table 2). Neither rate showed significant differences (p >0.05) between spring-summer 2020–2021 (Figure 8a) and summer of 2022 (Figure 8b). Although there were no significant differences (p >0.05) between GPP values recorded from different fjords in both study periods (Figure 8a, 8b), Comau Fjord showed the lowest rates of GPP (0.1 to 0.6 g C m^{-2} d^{-1}) whereas Puyuhuapi and Reloncaví fjords showed the highest values (1.9 to 2.6 g C m^{-2} d^{-1}). In the case of CR, the highest rates were recorded in Puyuhuapi Fjord (2.2 to 6.6 g C m^{-2} d^{-1}) and the lowest in Comau Fjord (0.8 to 0.9 g C m^{-2} d^{-1}) (Figure 8a, 8b). The phytoplankton composition in the study area showed a similar pattern to the GPP values, highlighting maximum abundances on the surface and minimal abundances at a depth of 20 m (data not shown). In addition, Comau Fjord showed the lowest abundances (66 × 10^3 cell L^{-1}) whereas Reloncaví Fjord showed the highest concentrations of phytoplankton (1,227 × 10^3 cell L^{-1}).

Estimated rates of BSP ranged between 0.05 and 0.6 g C m^{-2} d^{-1} within the study area and were positively and significantly correlated with GPP values (Figure 8, Table 2). The percentage of GPP utilized by bacteria ranged

https://doi.org/10.5194/egusphere-2023-706
Preprint. Discussion started: 26 April 2023

from 3% to 56%, except in Comau Fjord, where a higher utilization percentage (151%) was recorded, suggesting that more organic carbon is consumed than is produced locally.

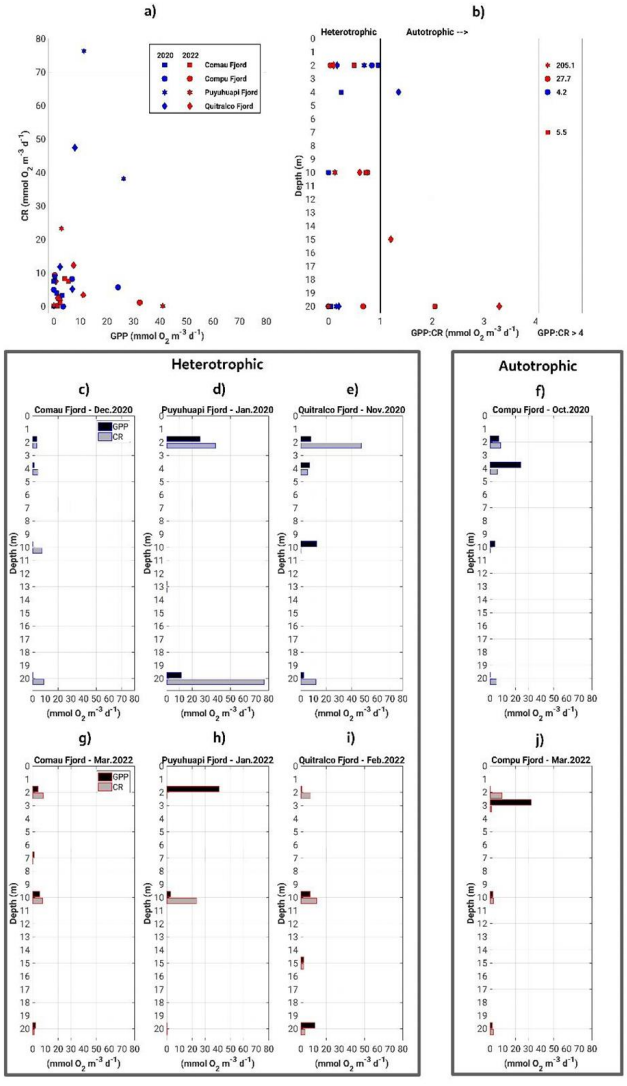

Figure 7. (a) Relationship and (b) vertical patterns of all datasets from the GPP and CR. (c−j) represents the vertical distribution of GPP and CR obtained during experiments of primary production on (c−f) spring-summer of 2020−2021, and (g−j) summer of 2022. GPP: Global primary production, and CR: community respiration.

https://doi.org/10.5194/egusphere-2023-706
Preprint. Discussion started: 26 April 2023

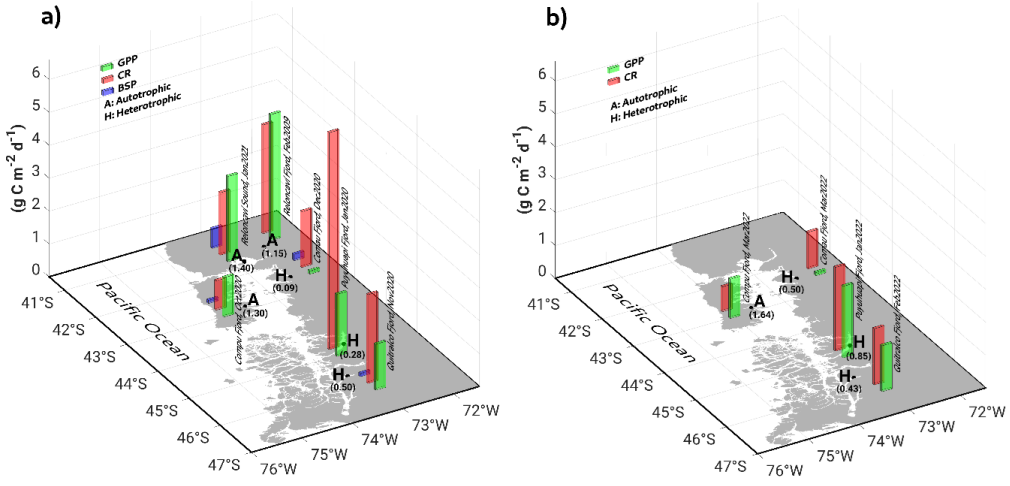

370 **Figure 8**. *In-situ* experiment of primary production during (a) spring-summer of 2020−2021, and (b) summer of 2022, covering some fjords in the northern Patagonian fjord system. GPP: Global primary production, CR: Community respiration, BSP: Bacterial secondary production. Results shown from Reloncaví Fjord in (a) were extracted from Montero et al., (2011).

375 3.3. Satellite image of organic matter supply to fjords

Satellite images show that freshwater inputs into the sea were accompanied by large amounts of suspended sediments (Figure 9), possibly acting as a source of allochthonous organic matter, favoring the heterotrophic metabolism reported in the previous section. On May 9, 2017, a large amount of suspended matter flowed into the Reloncaví Sound from its fjord, mainly dominated by three rivers: Petrohue, Cochamo, and Puelo (Figure 9a). In the 380 southeast part of the Reloncaví Sound, the observed high concentration of sediments was due to the presence of a diatom bloom mainly formed by *Skeletonema costatum*, which attained concentrations of more than 5 million cells L^{-1} within the fjord (Figure not shown). This bloom affected both the eastern part of the Reloncaví Sound and the Reloncaví Fjord. While the amount of suspended matter visible in the Sentinel-2 images was generally homogeneously high along the fjords e.g., on June 9, 2022, in the Quitralco Fjord (Figure 9b), and May 9, 2017, in Reloncaví, (Figure 385 9a). Some examples of this phenomenon, such as the one on April 6, 2018, on Comau Fjord (Figure 9c), show a very heterogeneous distribution of suspended sediments within the fjord, suggesting the influence of the currents in the distribution of waters rich in sediment. On this date, waters flowing from the river Blanco in the northern part of the fjord's mouth were whitish in color, indicating carbonate-rich sediments. Water flowing into this fjord from the south, principally from the Lloncochaígua and Vodudahue rivers, has a more brownish color, indicating a higher quantity of 390 organic matter.

At the Quitralco Fjord (Figure 9b), suspended sediments from Rio de los Huemules (at 73.30° E 45.54° S, the brown riverbed is clearly visible in the natural color insert) appeared to propagate within the fjord, affecting the water clarity

https://doi.org/10.5194/egusphere-2023-706
Preprint. Discussion started: 26 April 2023

along the entire fjord. Inspection on other dates (not shown) revealed high variability in the direction of the river outflow, sometimes entering the fjord (and staying there for extended periods), and sometimes being directed towards the south. Finally, the Puyuhuapi Fjord also registered a high signal from suspended sediments due to river discharge; for example, the Vestiquero River was located at the fjord head (Figure 9d). Other rivers, such as the Cisnes, Marta, and Uspallante, could also influence the supply of allochthonous organic matter to the Puyuhuapi Fjord, contributing to a decrease in DO and hypoxia. However, the cloud cover does not allow for better satellite images.

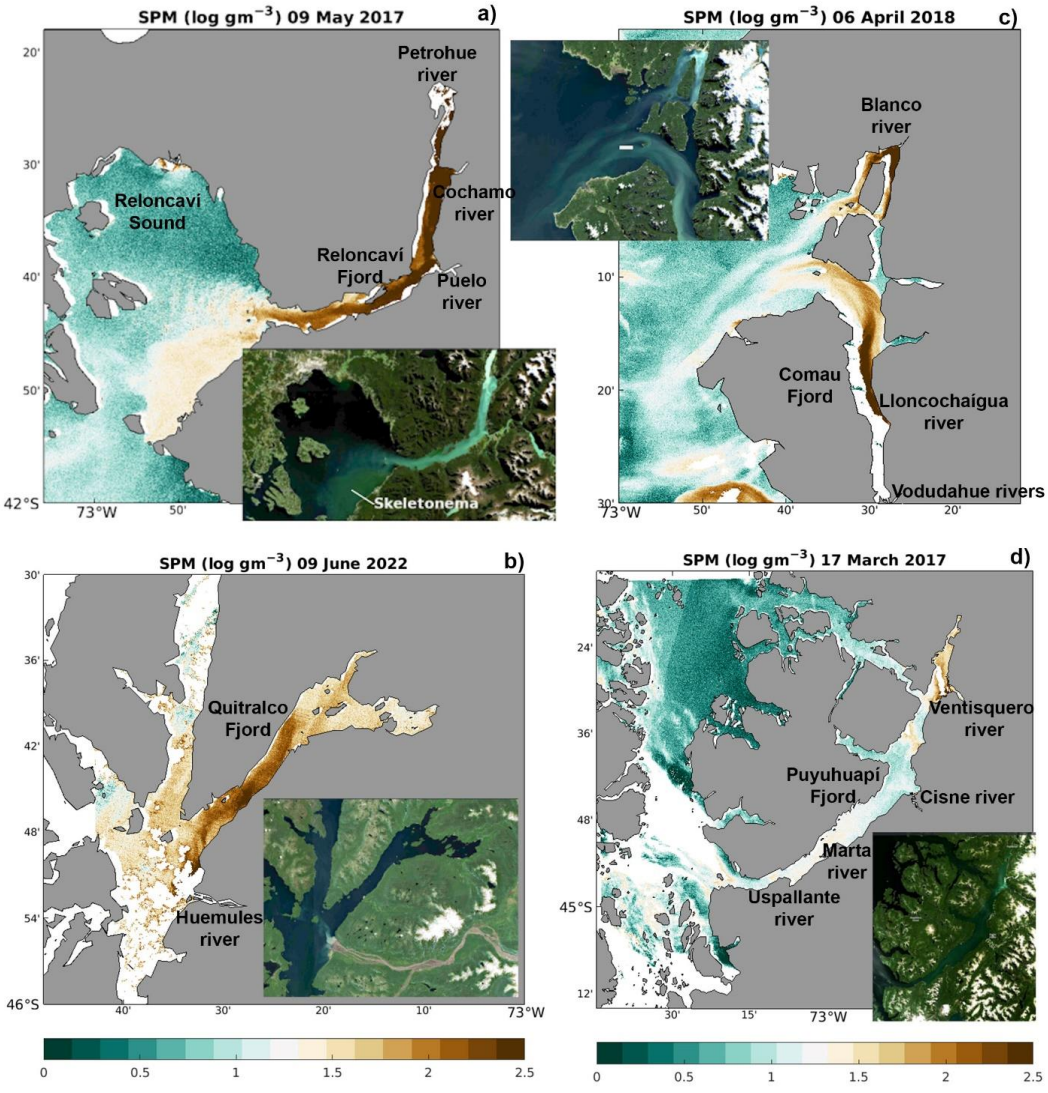

Figure 9. Suspended particulate matter as measured by Sentinel 2 on (a) Reloncaví Sound, (b) Quitralco Fjord, (c) Comau Fjord, and (d) Puyuhuapi Fjord.

https://doi.org/10.5194/egusphere-2023-706
Preprint. Discussion started: 26 April 2023

3.4. Biogeochemical parameters

South of the study area (Figure 10a), the suspended particulate matter (SPM) (Figure 10b) was high from Puyuhuapi Fjord to San Rafael Lagoon, with maximum values > 4 mg L^{-1}. In the north area, a little sub-surface core close to Comau Fjord and the Reloncaví system showed an increase in the SPM. The % of POM allochthonous (POM_{allo}) showed an irregular distribution (Figure 10c), with a subsurface minimum < 30% in the mouth of Quitralco, Aysén, and Puyuhuapi fjords in the south and, Comau and Reloncaví system in the north. The POM_{allo} increased with depth, reaching approximately 70%, except for the Chiloé Inner Sea, where POM_{allo} was less than 50%. The C:N ratio shows sub-surface values <8 at depths above 50 m (Figure 10d), and increasing values to depth greater than 15 m from Jacaf Channel to the San Rafael Lagoon. In the Chiloé Inner Sea, the autochthonous organic matter increased. The isotopic signal showed an increase in the same sites where the % POM_{allo} decreased, with values between -25‰ and -15‰. At depth, the organic matter showed light relative to the surface (Figure 10e). High nitrogen-enrichment values were evident at the surface level from the south of Chiloé Inner Sea to the Aysén Fjord (Figure 10f), showing a significant increase with values > 9% up to 150 m in the Chiloé Inner Sea. High concentrations of CDOM were observed north of the Patagonian fjords (Figure 10g) along all water columns. To the south of the study system, there was a decrease in CDOM concentration with minimum values as low as 20 ug L^{-1} SQU, from Jacaf Channel to San Rafael Lagoon.

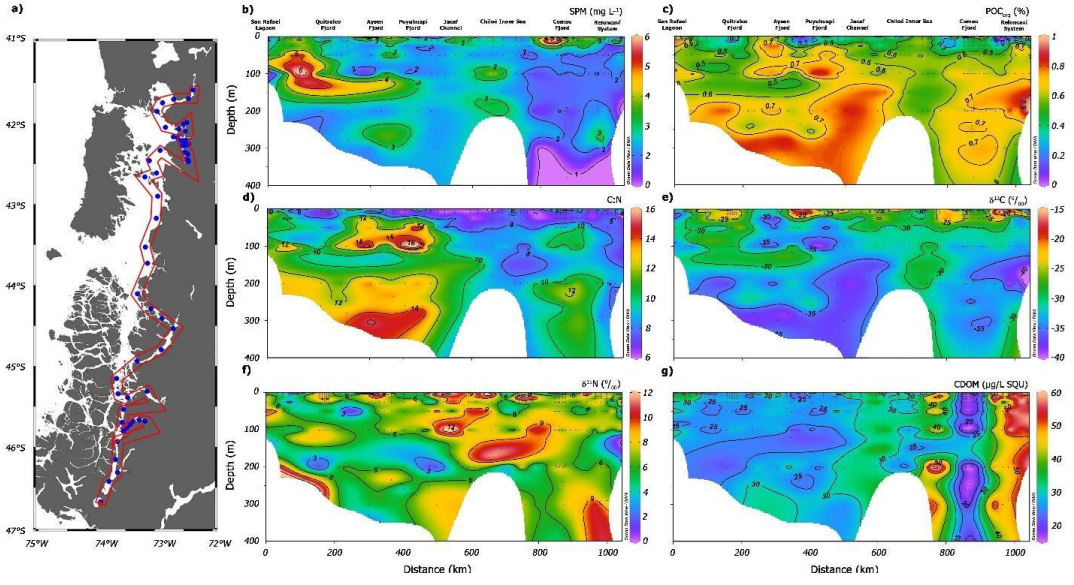

Figure 10. (a) Study area showing transect (red color) used to biogeochemical study case carried out in November 2020 during Expeditions PN-I IFOP. (b) Suspended particular material (SPM), (c) allochthonous carbon percentage

https://doi.org/10.5194/egusphere-2023-706
Preprint. Discussion started: 26 April 2023

(POC_{allo}), (d) Carbon and nitrogen ratio (C:N), Isotopic signal of (e) $\delta^{13}C$ and (f) $\delta^{15}N$, and (g) Chromophoric Dissolved Organic Matter (CDOM).

3.5. Circulation regime from ADCP measurements

The low-frequency deep circulation (> 40 m depth) in the inner sea of the region showed a marked east–west regional gradient in the along-channel current amplitude (Figure 11). The Corcovado currents were dominated by an eastward flow with a maximum intensity of approximately 30 cm s^{-1} (Figure 11a), whereas at the mouth of the Puyuhuapi Fjord (Figure 11b), the maximum current was approximately 10 cm s^{-1}.

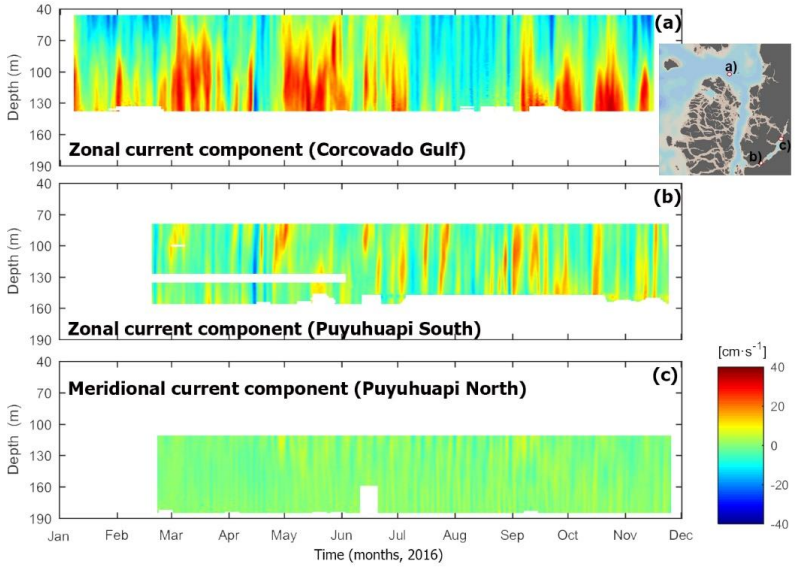

Figure 11. Subtidal deep circulation regimen obtained with ADCP performed in the (a) Corcovado Gulf and in (b, c) southern-northern zone of the Puyuhuapi Fjord from January to November 2016.

The Corcovado currents showed a marked pattern in the 40–70 m layer, which was dominated by westward currents, and short-duration events of approximately 20 cm s^{-1} were observed throughout the entire time series. This strong westward flow seems to be associated with the austral spring-summer seasons (January–March and November–December 2016); however, a weak (~5 cm s^{-1}) and longer (July–October 2016) westward flow was observed during the austral winter-autumn period. In the layer between 70 and 130 m, eastward (and strong) currents dominated, and there were periods of one to two months with eastward flow during March–April, May–July, and September–December 2016 with currents > 20 cm s^{-1}. The layer between 100 and 130 m showed maximum currents of approximately 40 cm s^{-1} at the end of October 2016 (Figure 11a).

Puyuhuapi Fjord currents were obtained at the southern mouth (South Puyuhuapi, Figure 11b) and middle fjord (North Puyuhuapi, Figure 11c). At the mouth of the fjord, low-frequency currents showed short pulses that covered most of the 70–160 m layer; typically, those pulses were eastward without an evident seasonal pattern. A

https://doi.org/10.5194/egusphere-2023-706
Preprint. Discussion started: 26 April 2023

unique low-frequency westward event was observed in mid-April 2016, which was also present in the Corcovado Gulf. In general, the currents in southern Puyuhuapi were weak (< 10 cm s^{-1}); however, during September and October 2016, eastward events of 20 cm s^{-1} were observed. In northern Puyuhuapi, most currents were weak (< 10 cm s^{-1}) without a temporally or spatially evident pattern, and the flow tended to be northward and intensified between May and September 2016.

3.6 Circulation regimen oceanographic model

Deep currents, defined as subtidal or residual currents (average of 50–300 m) over the three years of simulation, have a relatively large spatial variation. Consequently, the model could correlate the most energetic zones in the outer channels with those of lower energy inside the fjords. This result becomes clearer when looking at Figures 12a and 12b, which show the spatial variability of the net current speed. In general, the exchanges between the fjords and ocean registered high average velocities, that is, the Guafo mouth, Moraleda Channel, Corcovado Gulf, and Desertores Channel, with net current velocities ranging from 10 to 20 cm s^{-1}. In contrast, in the fjords, the average

https://doi.org/10.5194/egusphere-2023-706
Preprint. Discussion started: 26 April 2023

velocity of the deep current was less than 5 cm s^{-1}. The predominant flow was generally towards the interior of the fjords.

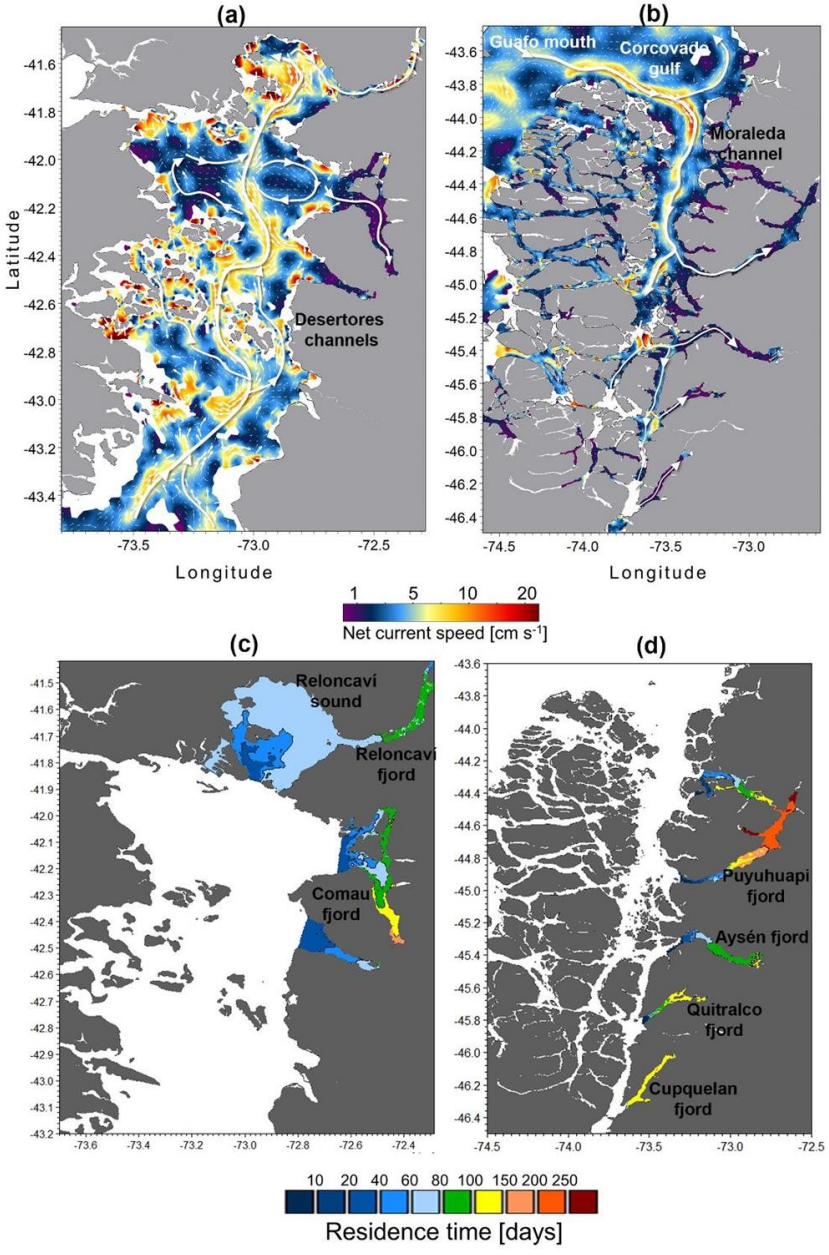

460

Figure 12. (a, b) Map showing the deep currents regime in northern Patagonian fjords. The deep current was defined as subtidal currents calculated as the average of currents from 50–300 m depth. (c, d) The residence time was

https://doi.org/10.5194/egusphere-2023-706
Preprint. Discussion started: 26 April 2023

calculated for each fjord of the northern Patagonian. (a-d) Data were obtained from the hydrodynamic model MIKE 3 FM developed by IFOP.

The flushing/residence time calculated for each fjord showed that the sector towards the head of Puyuhuapi Fjord registered the longest retention time (>200 days). In comparison, the shortest times were found in the Reloncaví Sound–Fjord (60–90 days), except for the Reloncaví Fjord head, which reached values close to 100 days (Figure 12c and 12d). Comau Fjord showed relatively high values, which increased from north to south. In the central part of Comau Fjord, the residence time ranged from 90 to 120 days, whereas at the fjord head, it ranged from 150 to 190 days. Meanwhile, the Aysén Fjord showed residence time values lower than 120 days, which were higher towards the fjord head, whereas the Quitralco Fjord reported 150 days at the fjord head and 100 days at its central part. Finally, the Cupquelán Fjord exhibited greater homogeneity throughout the fjord, with relatively high values ranging from 120 to 150 days. Most studies reported a spatial gradient of water retention, with the highest values found near the fjord's head.

4. Discussion

Oceanographic research in the Patagonian fjords started in 1995 with CIMAR-fjords project, supported by the Chilean Navy. As an oceanographic sampling strategy, Patagonia was divided into three zones, e.g., northern (41°–47° S), central (47°–53° S), and southern (53°–55.8° S) Patagonia, and the frequency of the cruises were primarily seasonal (Sievers, 2008). Moreover, some oceanographic cruises, such as the Hudson expedition in 1970, occurred in this zone (Table 1). The data collected through the CIMAR projects allowed us to understand the main physical (water mass quantification) and chemical (e.g., dissolved oxygen and inorganic nutrients) processes impacting this fjord system, such as the hypoxic conditions due to the influence of the ESSW (Sievers, 2008; Sievers and Silva, 2008; Silva, 2008; Silva and Vargas, 2014; Schneider et al., 2014; Pérez-Santos et a., 2014). Furthermore, other studies have contributed to the understanding of processes favoring hypoxia and the reduction of DO, such as primary production and community respiration, associated with the abundance of different phytoplankton species (Montero et al., 2011; 2017; Iriarte et al., 2018). Additionally, the development of hydrodynamic models helped to determine the areas where the water age was significantly high, for example, the Puyuhuapi Fjord (Pinilla et al., 2020), and where stronger mixing stratification occurred (Ruiz et al., 2021). Recently, satellite data from suspended sediments have allowed us to understand the supply of allochthonous organic matter to fjords due to river discharge. Therefore, this study scrutinized all processes contributing to the presence of water under hypoxic conditions and LDOW in the northern Patagonian fjords, as discussed in the next section.

4.1 Water masses proprieties and biogeochemical processes in northern Patagonian Fjords

Recent and historical hydrographic data collected from the Patagonian fjords, especially in the northern area, confirmed the presence of analogous water masses detected previously by the Hudson oceanographic cruise in 1970. EW, MSAAW, SAAW, and ESSW were recorded from the surface layer to the bottom (to a depth of approximately 500 m) (Figure 3 and Figure 6). Similar patterns were recognized in terms of the vertical-horizontal distributions,

https://doi.org/10.5194/egusphere-2023-706
Preprint. Discussion started: 26 April 2023

highlighting the location of the salty-hypoxic-LDOW and nutrient-rich waters associated with the ESSW in the Jacaf Channel and Puyuhuapi Fjord. On the other hand, the EW dominated in the southern area due to freshwater input from the San Rafael Lagoon, which is characterized by oxygenated waters due to its high solubility. Finally, SAAW and MSAAW covered the entire study area (Figure 2), as reported by Siever and Silva (2008), Schneider et al., 2014, Pérez-Santos et al., 2014, and Pinilla et al., (2020).

Vigorous vertical mixing was observed throughout the year in the Chiloé Inner Sea (Figure 5). In this area, the physical and biogeochemical parameters showed homogeneous values from the surface layer to the bottom (Figure 2 and Figure 3), indicating the presence of MSAAW (originating from mixing the SAAW with the EW). Furthermore, the calculation of the buoyancy frequency and potential energy anomalies using the output from the oceanographic model demonstrated that more robust mixing occurred in the Chiloé Inner Sea (Ruiz et al., 2021). This explains the importance of this area for DO production and redistribution in the northern Patagonian fjords.

Water masses in northern Patagonia have unique physicochemical properties (Sievers and Silva, 2008; Silva, 2008; Silva and Vargas, 2014; Schneider et al., 2014; Pérez-Santos et al., 2014). From a biogeochemical standpoint, there are no classifications of water masses in the Patagonian fjords, even though the biotic and abiotic processes that occur in every body of water respond to the biogeochemical cycles to some extent. In the case of northern Patagonian fjords, EW is rich in silicic acid because of the riverine supply (Silva and Vargas, 2014), with characteristic pulses at the surface layer that changes throughout the year due to the organisms' consumption (Montero et al., 2011), as observed in northern Patagonia, including the Chiloé Inner Sea (Figure 3). Similarly, organic matter production in the subsurface layers generates regions of high carbon concentration with an enriched isotopic signal of mainly autochthonous origin (Figure 10). Silva and Vargas (2014) reported an LDOW zone developed near the fjord heads (<178 µmoL L^{-1}) because of more significant allochthonous particulate organic matter inputs transported by local rivers (Figure 9). However, there was a mixture of organic materials, which is why the POM isotopic values were relatively lighter than those expected if the organic matter pool was autochthonous. In any case, the enhanced organic matter input (autochthonous or allochthonous) to the deep layer increased DO consumption owing to respiration and overwhelmed the oxygen supplied by horizontal advection.

The spatial gradients of $\delta^{13}C$ have been previously documented in estuarine and continental shelf waters in Patagonian fjords (Silva and Vargas, 2008; Gonzalez et al., 2010; Iriarte et al., 2018), but there is no evidence of gradient of nitrogen isotopic signals. Nevertheless, the pronounced phytoplankton bloom resulted in an enrichment of $\delta^{13}C$ in SPM (Figure 10), similar to observations made in other fjords around the world (Remeikaite-Nikiene et al., 2017). In the same way, the enrichment of $\delta^{15}N$ of SPM results in primary production evidence that, in at least some regions of the fjords, the isotopic signals it was of mainly autochthonous origin (Figure 10). We did not establish a clear spatial gradient of $\delta^{13}C$ and $\delta^{15}N$ values in the Patagonian fjords. The results strongly indicate that the cause of the variability in C and N isotope fractionation was biological processes as previously demonstrated by Savoye et al., (2003) where the co-variation of $\delta^{13}C$ and $\delta^{15}N$ with seasonally changing abiotic factors, like temperature and nutrient concentrations, establishes the seasonal nature of $\delta^{13}C$ and $\delta^{15}N$ values as observed by reflecting the seasonal succession of phytoplankton species.

https://doi.org/10.5194/egusphere-2023-706
Preprint. Discussion started: 26 April 2023

The oceanic water masses (ESSW and SAAW) are strongly connected with the estuarine water masses (MSAAW and EW), as observed in this study (Figure 2). Organic matter degradation processes occurred inside the fjords, mainly in terms of nitrogenous compounds being remineralized, maintaining the nutrient pool that was originally transported by oceanic water, justifying the high accumulation of nitrate and phosphate registered in the subsurface layer of the Puyuhuapi Fjord and Jacaf Channel (Figure 3a-d). This process seems to be even more evident from the Jacaf Channel to the south (Figure 3), where it seems that organic matter was mostly retained and sedimented, which probably generated zones more prone to LDOW and hypoxia (Figure 2 and Figure 3).

At the fjord heads, where low salinity from high river freshwater inputs dominated, a persistent halocline/pycnocline/stratified water column developed; therefore, deep-water ventilation by vertical mixing and diffusion with the oxic surface layer was limited (Figure 2–5). These conditions favored the occurrence of LDOW zones at the fjord, where stratification and particulate organic matter input were higher than at their mouths (Figure 9), thus favoring the consumption of DO due to organic matter degradation, as was reported in the Milford Sound in New Zealand (Stanton, 1984), Framvaren Fjord in Norway (Yao and Millero, 1995) and the Lower St. Lawrence Estuary in Canada (Lefort et al., 2012), as well as in the Reloncaví, Comau, Puyuhuapi, Aysén, and Quitralco fjords (Figure 2).

4.2. Mechanisms driving hypoxia and deoxygenation in northern Patagonian fjords

As discussed in the previous section, one of the principal mechanisms involved in the origin of hypoxic conditions in some areas of the northern Patagonian fjords was attributed to the advection of the ESSW from the Pacific Ocean to Patagonia. Recently, Linford et al. (2023) demonstrated the poleward advection of water with lower DO values by the ESSW that was transported by the Perú Chile Undercurrent (PCUC). The passage of this water mass into the northern Patagonian fjord system was detected in a DO time series from a mooring system installed at the Guafo mouth. Moreover, as shown in Figure 2, extreme hypoxic conditions were registered in the Quitralco Fjord, where ESSW was not delivered (Figure 4d-f).

In the Quitralco Fjord, the DO concentration was mainly governed by the biological processes of oxygen production and consumption during photosynthesis and respiration, respectively. The primary production experiments conducted in this fjord (Figure 7 and Figure 8) showed higher values of community respiration than the primary production of DO (Table 2). In addition, the oceanographic model showed a less intense deep net current, allowing a residence time of water between 100−150 days (Figures 11 and 12). Furthermore, satellite images provide evidence of highly suspended sediments along the Quitralco Fjord due to river discharge (Figure 9).

DO produced by photosynthesis is primarily depleted through respiration; therefore, in many oceanic environments, the GPP and CR rates tend to be tightly coupled. However, in coastal waters or fjord ecosystems, owing to the high amount of organic matter (autochthonous and allochthonous) available in the water column, a greater amount of oxygen is consumed during microbial respiration (Robinson, 2019), thus dominating heterotrophic processes over autotrophic processes. This study recorded high CR rates (greater GPP), indicating heterotrophic metabolism, where more oxygen was consumed than produced (Figure 7). Nevertheless, Puyuhuapi, Reloncaví, and Compu fjords always showed high oxygen production values (GPP >20 mmol O_2 m^{-3} d^{-1}) at 2 m depth (Figure 8),

https://doi.org/10.5194/egusphere-2023-706
Preprint. Discussion started: 26 April 2023

confirming that Patagonian fjords act as a net sink of atmospheric CO_2 due to the high surface primary production rates (Torres et al., 2011). DO and organic matter are produced only in the well-lit upper ocean but can be consumed throughout the water column. Therefore, in areas of high surface production and slow resupply of oxygen at depth (compared to the rate at which oxygen is respired), DO concentrations may be reduced to hypoxic levels at depth.

However, the first map of residence time in the northern Patagonian fjord showed a coincidence of the area where a high residence time was reported (100–250 days, Figure 12) with the depleted oxygen region, for example, hypoxic and LDOW areas. The hydrodynamic model and derived calculations are helpful tools for explaining the oxygen distribution and patterns in the northern Patagonian fjord system.

Deoxygenation of subsurface water (50–200 m depth) was detected in Puyuhuapi Fjord when *in-situ* DO profiles were compared with a time-difference of 50 years, reporting negative values ΔDO = 30–40 µmol L^{-1} (Figure 6). Linford et al. (2023) provided an explanation for deoxygenation in Patagonian waters. The leading causes were the increase in the poleward transport of the PCUC and the consequent increase in the advection of the ESSW to the Patagonian. Moreover, as presented in this manuscript, we also included evidence of the biological-physical processes (DO consumption during respiration, lower ventilation, and suspended sediment supply) as one of the other processes contributing to deoxygenation in Patagonian fjords. In addition, an increase in inorganic nutrients, e.g., NO^3 and PO_4 of 2 µM and 0.5 µM was also registered in the last 50 years, possibly due to the increase in the primary production or as a response to anthropogenic activities, e.g., salmon and mussel aquaculture. However, further investigation is necessary to quantify the impact of these economic activities on the deoxygenation process.

5. Conclusions

Since the beginning of oceanographic research in the Patagonian fjords (1970), hypoxia and LDOW have been reported along the water column. A dataset of hydrographic-biogeochemical parameters, *in-situ* experiments of primary production/community respiration, satellite-suspended sediments, and the output of a hydrodynamic model allowed for the first time the quantification of the oceanographic processes contributing to the hypoxia and deoxygenation of the Patagonian subsurface water. The influence of the ESSW was recognized as one of the first drivers of this phenomenon. This water mass transported poleward poorly oxygenated waters that entered the northern Patagonian fjords through the Guafo mouth and moved southward through the Moraleda and Jacaf channels and the Puyuhuapi fjord. The distribution of the ESSW inside the northern Patagonian fjords coincides with the most extensive zone of the LDOW records. However, the hypoxic conditions registered in this zone were also attributed to the high rate of DO consumption during community respiration processes, owing to the entrance of allochthonous organic matter (natural and/or anthropogenic) to the fjords. Additionally, the results from marine currents derived from ADCP measurements and the hydrodynamic model demonstrated a weak water circulation and a long residence time contributing to the reduction of deep-water ventilation, resulting in a drop in DO level, and finally, the occurrence of hypoxic conditions.

The Quitralco Fjord also reported hypoxic conditions showing the absolute minimum of DO with 9.36 µmol L^{-1} and 1.6% oxygen saturation. ESSW was not observed in this area. Therefore, the presence of hypoxic water in the deep layer of Quitralco was attributed to weak deep-water circulation and a long residence time, together with a high rate of DO consumption by community respiration and a higher supply of allochthonous organic matter due to river

https://doi.org/10.5194/egusphere-2023-706
Preprint. Discussion started: 26 April 2023

discharge. Similar processes favoring LDOW were registered at the Aysén, Comau, and Reloncaví fjords, but in the Reloncaví systems, marine currents and residence time were significantly higher than in other fjords. The presence of LDOW in the Reloncaví systems responded mainly to biological processes, e.g., DO consumption during the primary production by phytoplankton, and secondary production by bacteria.

Quantification of the processes contributing to hypoxic conditions and LDOW in the water column of northern Patagonian fjords allowed for the identification of the main causes favoring the deoxygenation of each fjord investigated. The results provide the environmental information needed to contribute to the sustainable management of the northern Patagonian fjord under anthropogenic activities and climate change scenarios. In addition, it provides significant information for understanding the life cycle of marine species that inhabit Patagonian fjords.

Data availability. All data sets used in this manuscript can be requested from the corresponding author.

Author contributions. PL: study design, data analysis, and manuscript leader. IPS: study design, collection, and analysis of physical oceanographic data, and manuscript leader. PM: study design, collection, and analysis of primary production data. PD: study design, collection, and analysis of physical-biological oceanographic data. CA: collection, and analysis of primary production data. EP: developed of oceanographic model and analysis of physical oceanographic data. FB: collection, and analysis of biogeochemical data. MC: analysis of marine current data. AA: study design, collection, and analysis of satellite data. MA: collection and analysis of marine current data. GS: study design, collection, and analysis of physical oceanographic data. CP: edition and analysis of satellite data. CS: collection, and analysis of physical oceanographic data. SA: collection, and analysis of biogeochemical data. PN: collection, and analysis of biogeochemical data. GM: collection of physical, biological, and biogeochemical data. RA: collection of physical, biological, and biogeochemical data. JSM: processing and analysis of model data for resident time. CSR: validation hydrodynamics model. All authors contributed to the writing of the manuscript.

Competing interests. The authors declare that they have no conflict of interest.

Acknowledgments.

This research was funded by COPAS Sur-Austral ANID AFB170006, the Office of Naval Research grant N00014-17-1-2606, COPAS COASTAL FB210021, and CIEP R20F002. Iván Pérez-Santos was also funded by FONDECYT 1211037. Facundo Barrera was founded by FONDECYT 31308. Cécile Pujol was financially supported by the F.R.S-FNRS (Fonds de la Recherche Scientifique de Belgique, Communauté Française de Belgique) through a FRIA grant. Patricio A. Díaz was funded by Centre for Biotechnology and Bioengineering (CeBiB) (PIA project FB0001, ANID, Chile). M.I. Castillo was funded by CS2018-7929 and ATE220033. We also thank the Chonos initiative of the Instituto de Fomento Pesquero (IFOP) for facilitating the use of its computer systems to access the MIKE 3, WRF, and FLOW models and the Ministry of Economy, Development and Tourism of the Chilean Government for funding through the Undersecretary of Fisheries and Aquaculture. Elias Pinilla would like to acknowledge funding from the National Science Foundation (NSF Grant Number 2045866).

https://doi.org/10.5194/egusphere-2023-706
Preprint. Discussion started: 26 April 2023

Andrejev, O., Myrberg, K., and Lundberg, P. A.: Age and renewal time of water masses in a semi-enclosed basin—application to the Gulf of Finland, Tellus A: Dynamic Meteorology and Oceanography, 56, 5 , 548-558, doi:10.3402/tellusa.v56i5.14435, 2004.

Andrewartha, H. G., and Birch, L. C.: The ecological web: more on the distribution and abundance of animals, University of Chicago Press, 1986.

Barrera, F., Lara ,R. Krock, J., Factors influencing characteristics and distribution of organic particles and macromolecules in the Pacific-Atlantic connection, J. Mar. Syst., 175, 36-45, doi:10.1016/j.jmarsys.2017.07.004, 2017.

Batiuk, R. A., Breitburg, D. L., Diaz, R. J., Cronin, T. M., Secor, D. H., and Thursby, G.: Derivation of habitat-specific dissolved oxygen criteria for Chesapeake Bay and its tidal tributaries, Journal of Experimental Marine Biology and Ecology, 381, S204-S215, doi:10.1016/j.jembe.2009.07.023, 2009.

Bianchi, T. S.: Biogeochemistry of estuaries. Oxford University Press on Demand, 2007.

Billi, M., Mascareño, A., Henríquez, P. A., Rodríguez, I., Padilla, F., and Ruz, G. A.: Learning from crises? The long and winding road of the salmon industry in Chiloé Island, Chile, Marine Policy, 140, 105069, doi:10.16/j.marpol.2022.105069, 2022.

Breitburg, D. L., Loher, T., Pacey, C. A., and Gerstein, A.: Varying effects of low dissolved oxygen on trophic interactions in an estuarine food web, Ecological Monographs, 67, 4, 489-507, doi:10.1890/0012-9615(1997)067[0489:VEOLDO]2.0.CO;2, 1997.

Breitburg, D., Levin, L. A., Oschlies, A., Grégoire, M., Chavez, F. P., Conley, D. J., ... and Zhang, J.: Declining oxygen in the global ocean and coastal waters, Science, 359, 6371, doi:10.1126/science.aam7240, 2018.

Castillo, M. I., Cifuentes, U., Pizarro, O., Djurfeldt, L., and Caceres, M.: Seasonal hydrography and surface outflow in a fjord with a deep sill: the Reloncaví fjord, Chile, Ocean Science, 12, 2, 533-544, doi:10.5194/os-12-533-2016, 2016.

Conley, D. J., Paerl, H. W., Howarth, R. W., Boesch, D. F., Seitzinger, S. P., Havens, K. E., ... and Likens, G. E.: Controlling eutrophication: nitrogen and phosphorus, Science, 323, 5917, 1014-1015, doi:10.1126/science.1167755, 2009.

Davis, J. C.: Minimal dissolved oxygen requirements of aquatic life with emphasis on Canadian species: a review, Journal of the Fisheries Board of Canada, 32, 12, 2295-2332, doi:10.1139/f75-268, 1975.

Diaz, R. J., and Rosenberg, R.: Marine benthic hypoxia: a review of its ecological effects and the behavioural responses of benthic macrofauna, Oceanography and marine biology, An annual review, 33, 245, 03, 1995.

Diaz, R. J.: Overview of hypoxia around the world, Journal of environmental quality, 30, 2, 275-281, doi:10.2134/jeq2001.302275x, 2001.

Díaz, P. A., Pérez-Santos, I., Basti, L., Garreaud, R., Pinilla, E., Barrera, F., ... and Figueroa, R. I.: The impact of local and climate change drivers on the formation, dynamics, and potential recurrence of a massive fish-killing microalgal bloom in Patagonian fjord, Science of The Total Environment, 865, 161288, doi:10.16/j.scitotenv.2022.161288, 2023.

https://doi.org/10.5194/egusphere-2023-706
Preprint. Discussion started: 26 April 2023

Ekau, W., Auel, H., Pörtner, H. O., and Gilbert, D.: Impacts of hypoxia on the structure and processes in pelagic communities (zooplankton, macro-invertebrates and fish), Biogeosciences, 7, 5, doi:10.5194/bg-7-1669-2010, 1669-1699, 2010.

Fuenzalida, R., Schneider, W., Garcés-Vargas, J., Bravo, L., and Lange, C. : Vertical and horizontal extension of the oxygen minimum zone in the eastern South Pacific Ocean, Deep Sea Research Part II: Topical Studies in Oceanography, 56, 16, 992-1003, doi:10.1016/j.dsr2.2008.11.001, 2009.

Garcon V., Dewitte B., Goubanova C. and Montes I.: Land-sea-atmosphere interactions exacerbating ocean deoxygenation in Eastern Boundary Upwelling Systems (EBUS), in 'Laffoley, D. and Baxter, J.M. (eds.). Ocean deoxygenation: Everyone's problem - Causes, impacts, consequences and solutions, Gland, Switzerland: IUCN. xxii+562pp, available at: https://portals. iucn. org/library/sites/library/files/documents/03.420 DEOX. Pdf, 2019.

González, H. E., Calderón, M. J., Castro, L., Clement, A., Cuevas, L. A., Daneri, G., ... and Molinet, C.: Primary production and plankton dynamics in the Reloncaví Fjord and the Interior Sea of Chiloé, Northern Patagonia, Chile, Marine Ecology Progress Series, 402, 13-30, doi:10.3354/meps08360, 2010.

González, H. E., Nimptsch, J., Giesecke, R., and Silva, N.: Organic matter distribution, composition and its possible fate in the Chilean North-Patagonian estuarine system, Science of the Total Environment, 657, 1419-1431, doi:10.1016/j.scitotenv.2018.11.445, 2019.

Grasshoff, K., Ehrhardt, M., and Kremling, K. Methods of Seawater Analysis. (2nd edition), Verlag Chemie Weinhein, New York, USA, 1983.

Grasshoff, K., Kremling, K., and Ehrhardt, M. (Eds.).: Methods of seawater analysis, John Wiley and Sons, 2009.

Herrmann, R. B.: Growth of juvenile coho salmon at various concentrations of dissolved oxygen, 1958.

Hoos, L.M.: A study of the benthos of an anoxic marine basin and factors affecting its distribution, M. Sc. Thesis, Dalhousie University, Halifax, NS. 149, 1973.

IOC, S.: IAPSO: The international thermodynamic equation of seawater–2010: Calculation and use of thermodynamic properties, Intergovernmental Oceanographic Commission, Manuals and Guides No. 56, UNESCO, Manuals and Guides, 56, 1-196, 2010.

Iriarte, J. L.: Natural and human influences on marine processes in Patagonian Subantarctic coastal waters, Frontiers in Marine Science, 5, 360, doi:10.3389/fmars.2018.00360, 2018.

Kattner, G., and Becker, H.: Nutrients and organic nitrogenous compounds in the marginal ice zone of the Fram Strait, Journal of Marine Systems, 2, 3-4, 385-394, doi:10.1016/0924-7963(91)90043-T, 1991.

Kutty, M. N.: Respiratory quotients in goldfish and rainbow trout, Journal of the Fisheries Board of Canada, 25, 8, 1689-1728, doi:10.1139/f68-150, 1968.

Laffoley, D., and Baxter, J. M.: Ocean deoxygenation: Everyone's problem-Causes, impacts, consequences and solutions, Gland, Switzerland: IUCN, doi:10.2305/IUCN.CH.2019.13.en, 2019.

Lefort, S.: A multidisciplinary study of hypoxia in the deep water of the Estuary and Gulf of St. Lawrence: Is this ecosystem on borrowed time?, McGill University (Canada), 2012.

Linford, P., Pérez-Santos, I., Montes, I., Dewitte, B., Buchan, S., Narváez, D., Saldías, G., Pinilla, E., Garreaud, R., Díaz, P., Schwerter, C., Montero, P., Rodríguez-Villegas, C., Cáceres-Soto, M., Mancilla-Gutiérrez, G., and

https://doi.org/10.5194/egusphere-2023-706
Preprint. Discussion started: 26 April 2023

720 Altamirano R.: Recent Deoxygenation of Patagonian Fjord Subsurface Waters Connected to the Peru–Chile Undercurrent and Equatorial Subsurface Water Variability. Submitted to Global Biogeochemical cycles (Under review), 2023.

Martínez, D., De Lázaro, O., Cortés, P., Oyarzún-Salazar, R., Paschke, K., and Vargas-Chacoff, L.: Hypoxia modulates the transcriptional immunological response in Oncorhynchus kisutch, Fish and Shellfish Immunology, 106, 725 1042-1051, doi:10.16/j.fsi.2020.09.025, 2020.

Meire, L. K. E. R., Soetaert, K. E. R., and Meysman, F. J. R.: Impact of global change on coastal oxygen dynamics and risk of hypoxia, Biogeosciences, 10, 4, 2633-2653, doi:10.5194/bg-10-2633-2013, 2013.

Monsen, N. E., Cloern, J. E., Lucas, L. V., and Monismith, S. G.: A comment on the use of flushing time, residence time, and age as transport time scales, Limnology and oceanography, 47, 5, 1545-1553, 730 doi:10.4319/lo.2002.47.5.1545, 2002.

Montero, P., Daneri, G., Gonzalez, H. E., Iriarte, J. L., Tapia, F. J., Lizarraga, L., ... and Pizarro, O.: Seasonal variability of primary production in a fjord ecosystem of the Chilean Patagonia: Implications for the transfer of carbon within pelagic food webs, Continental Shelf Research, 31, 3-4, 202-215, doi:10.1016/j.csr.2010.09.003, 2011.

Montero, P., Pérez-Santos, I., Daneri, G., Gutiérrez, M. H., Igor, G., Seguel, R., ... and Crawford, D. W.: A winter 735 dinoflagellate bloom drives high rates of primary production in a Patagonian fjord ecosystem, Estuarine, Coastal and Shelf Science, 199, 105-116, doi:10.3856/vol45-issue5-fulltext-16, 2017.

Montero, P., Daneri, G., Tapia, F., Iriarte, J. L., and Crawford, D.: Diatom blooms and primary production in a channel ecosystem of central Patagonia, Lat. Am. J. Aquat. Res. 45, 999–1016, doi: 10.3856/vol45-issue5-fulltext-16, 2017a.

Montero, P., Gutiérrez, M. H., Daneri, G., and Jacob, B.: The Effect of Salmon Food-Derived DOM and Glacial 740 Melting on Activity and Diversity of Free-Living Bacterioplankton in Chilean Patagonian Fjords, Frontiers in Microbiology, 12, 772900, doi:10.3389/fmicb.2021.772900, 2022.

Nechad, B., Dogliotti, A., Ruddick, K., and Doxaran, D.: Particulate backscattering and suspended matter concentration retrieval from remote-sensed turbidity in various coastal and riverine turbid waters, In Living Planet Symposium, Proceedings of the conference held, 9-13, 2016.

745 Nimptsch, J., Woelfl, S., Osorio, S., Valenzuela, J., Ebersbach, P., von Tuempling, W., ... and Graeber, D.: Tracing dissolved organic matter (DOM) from land-based aquaculture systems in North Patagonian streams, Science of the Total Environment, 537, 129-138, doi:10.1016/j.scitotenv.2015.07.160, 2015.

Oschlies, A., Brandt, P., Stramma, L., and Schmidtko, S.: Drivers and mechanisms of ocean deoxygenation, Nature Geoscience, 11, 7, 467-473, doi:10.1038/s41561-018-0152-1, 2018.

750 Paulmier, A., and Ruiz-Pino, D.: Oxygen minimum zones (OMZs) in the modern ocean, Progress in Oceanography, 80, 3-4, 113-128, doi:10.1016/j.pocean.2008.08.001, 2009.

Pérez-Santos, I., Garcés-Vargas, J., Schneider, W., Ross, L., Parra, S., and Valle-Levinson, A.: Double-diffusive layering and mixing in Patagonian fjords, Progress in Oceanography, 129, 35-49, doi:10.1016/j.pocean.2014.03.012, 2014.

https://doi.org/10.5194/egusphere-2023-706
Preprint. Discussion started: 26 April 2023

Pérez-Santos, I., Castro, L., Ross, L., Niklitschek, E., Mayorga, N., Cubillos, L., ... and Daneri, G.: Turbulence and hypoxia contribute to dense biological scattering layers in a Patagonian fjord system, Ocean Science, 14, 5, 1185-1206, doi:10.5194/os-14-1185-2018, 2018.

Pinilla, E., Castillo, M. I., Pérez-Santos, I., Venegas, O., and Valle-Levinson, A.: Water age variability in a Patagonian fjord, Journal of Marine Systems, 210, 103376, doi:10.1016/j.jmarsys.2020.103376, 2020.

Prandle, D.: Simple theory for designing tidal power schemes, Advances in water resources, 7, 1, 21-27, doi:10.1016/0309-1708(84)90026-5, 1984.

Quiñones, R. A., Fuentes, M., Montes, R. M., Soto, D., and León-Muñoz, J.: Environmental issues in Chilean salmon farming: a review, Reviews in Aquaculture, 11, 2, 375-402, doi:10.1111/raq.12337, 2019.

Remeikaitė-Nikienė, N., Lujanienė, G., Malejevas, V., Barisevičiūtė, R., Zilius, M., Vybernaitė-Lubienė, I., ... and Stankevičius, A.: Assessing nature and dynamics of POM in transitional environment (the Curonian Lagoon, SE Baltic Sea) using a stable isotope approach, Ecological Indicators, 82, 217-226, doi:10.1016/j.ecolind.2017.06.035, 2017.

Robinson, C.: Microbial respiration, the engine of ocean deoxygenation, Frontiers in Marine Science, 5, 533, doi:10.3389/fmars.2018.00533, 2019.

Ruiz, C., Artal, O., Pinilla, E., and Sepúlveda, H. H.: Stratification and mixing in the Chilean Inland Sea using an operational model, Ocean Modelling, 158, 101750, doi:10.1016/j.ocemod.2020.101750, 2021.

Sampaio, E., Santos, C., Rosa, I. C., Ferreira, V., Pörtner, H. O., Duarte, C. M., ... and Rosa, R.: Impacts of hypoxic events surpass those of future ocean warming and acidification, Nature Ecology and Evolution, 5, 3, 311-321, doi:10.1038/s41559-020-01370-3, 2021.

Schmidtko, S., Stramma, L., and Visbeck, M.: Decline in global oceanic oxygen content during the past five decades, Nature, 542, 7641, 335-339, doi:10.1038/nature21399, 2017.

Schneider, W., Pérez-Santos, I., Ross, L., Bravo, L., Seguel, R., and Hernández, F.: On the hydrography of Puyuhuapi Channel, Chilean Patagonia, Progress in Oceanography, 129, 8-18, doi:10.1016/j.pocean.2014.03.007, 2014.

Sibson, R., and Thomson, G. D.: A seamed quadratic element for contouring, The Computer Journal, 24, 4, 378-382, doi:10.1093/comjnl/24.4.378, 1981.

Sievers, H. A.: Temperature and salinity in the austral Chilean channels and fjords. Progress in the oceanographic knowledge of Chilean interior waters, from Puerto Montt to Cape Horn. Comité Oceanográfico Nacional-Pontificia Universidad Católica de Valparaíso, Valparaíso, 31-36, 2008.

Sievers, A.H. and N. Silva.: Water masses and circulation in austral Chilean channels and fjords, In: N. Silva and S. Palma (eds.), Progress in the oceanographic knowledge of Chilean inner waters, from Puerto Montt to Cape Horn, Comité Oceanografico Nacional, Pontificia Universidad Católica de Valparaíso, Valparaíso, pp. 53-58. http://www.cona.cl/, 2008.

Silva, N.: Physical and chemical characteristics of the surface sediments in the austral Chilean channels and fjords, Progress in the oceanographic knowledge of Chilean interior waters, from Puerto Montt to Cape Horn, 69-75, http://www.cona.mil.cl/, 2008.

https://doi.org/10.5194/egusphere-2023-706
Preprint. Discussion started: 26 April 2023

Silva, N., Rojas, N., and Fedele, A.: Water masses in the Humboldt Current System: Properties, distribution, and the nitrate deficit as a chemical water mass tracer for Equatorial Subsurface Water off Chile, Deep Sea Research Part II: Topical Studies in Oceanography, 56, 16, 1004-1020, doi:10.1016/j.dsr2.2008.12.013, 2009.

Silva, N., and Vargas, C. A.: Hypoxia in Chilean patagonian fjords, Progress in Oceanography, 129, 62-74, doi:10.1016/j.pocean.2014.05.016, 2014.

Smith, D. C., and Azam, F.: A simple, economical method for measuring bacterial protein synthesis rates in seawater using 3H-leucine, Mar. Microb. food webs, 6, 2, 107-114, 1992.

Soto, D., and Norambuena, F.: Evaluation of salmon farming effects on marine systems in the inner seas of southern Chile: a large-scale mensurative experiment, Journal of Applied Ichthyology, 20, 6, 493-501, doi:10.1111/j.1439-0426.2004.00602, 2004.

Soto, D., León-Muñoz, J., Garreaud, R., Quiñones, R. A., and Morey, F.: Scientific warnings could help to reduce farmed salmon mortality due to harmful algal blooms, Marine Policy, 132, 104705, doi:10.16/j.marpol.2021.104705, 2021.

Stanton, B. R.: Some oceanographic observations in the New Zealand fjords, Estuarine, coastal and shelf science, 19, 1, 89-104, doi:10.1016/0272-7714(84)90054-4, 1984.

Strickland, J. D. H.: Measuring the production of marine phytoplankton, Fish. Res. Bd. Canada Bull., 122, 172, 1960.

Strickland, J. D. H., and Parsons, T. E.: Determination of dissolved oxygen, A practical handbook of seawater analysis, 167, 71-75, 1968.

Takeoka, H.: Fundamental concepts of exchange and transport time scales in a coastal sea, Continental Shelf Research, 3, 3, 311-326, doi:10.1016/0278-4343(84)90014-1, 1984.

Tomas, C. R. (Ed.).: Identifying marine phytoplankton, Elsevier, 1997

Torres, R., Pantoja, S., Harada, N., González, H. E., Daneri, G., Frangopulos, M., ... and Fukasawa, M.: Air-sea CO2 fluxes along the coast of Chile: From CO2 outgassing in central northern upwelling waters to CO2 uptake in southern Patagonian fjords, Journal of Geophysical Research: Oceans, 116, C9, doi:10.1029/2010JC006344, 2011.

Utermöhl, H.: Zur vervollkommnung der quantitativen phytoplankton-methodik: Mit 1 Tabelle und 15 abbildungen im Text und auf 1 Tafel, Internationale Vereinigung für theoretische und angewandte Limnologie: Mitteilungen, 9, 1, 1-38, doi:10.1018/05384680.1958.11904091, 1958.

Vanhellemont, Q., and Ruddick, K.: Atmospheric correction of metre-scale optical satellite data for inland and coastal water applications, Remote sensing of environment, 216, 586-597, doi:10.1016/j.rse.2018.07.015, 2018.

Vaquer-Sunyer, R., and Duarte, C. M.: Thresholds of hypoxia for marine biodiversity, Proceedings of the National Academy of Sciences, 105, 40, 15452-15457, doi:10.1073/pnas.0803833105, 2008.

Verardo, D. J., Froelich, P. N., and McIntyre, A.: Determination of organic carbon and nitrogen in marine sediments using the Carlo Erba NA-1500 Analyzer, Deep Sea Research Part A. Oceanographic Research Papers, 37, 1, 157-165, doi:10.1016/0198-0149(90)90034-S, 1990.

Wang, X., Olsen, L. M., Reitan, K. I., and Olsen, Y.: Discharge of nutrient wastes from salmon farms: environmental effects, and potential for integrated multi-trophic aquaculture, Aquaculture Environment Interactions, 2, 3, 267-283, doi:10.3354/aei00044, 2012.

https://doi.org/10.5194/egusphere-2023-706
Preprint. Discussion started: 26 April 2023

Williams, P. I., and Robertson, J. E.: Overall planktonic oxygen and carbon dioxide metabolisms: the problem of reconciling observations and calculations of photosynthetic quotients, Journal of plankton Research, 13, 153-169, doi:10.1093/oxfordjournals.plankt.a042366, 1991.

Yao, W., and Millero, F. J.: The chemistry of the anoxic waters in the Framvaren Fjord, Norway, Aquatic Geochemistry, 1, 53-88, 1995.